Chemical Engineering Journal 455 (2023) 140461

Contents lists available at ScienceDirect

Chemical Engineering Journal

journal homepage: www.elsevier.com/locate/cej

Review

Recent advances of photocatalytic degradation for BTEX: Materials, operation, and mechanism

Caixia Liang [a,b], Caiting Li [a,b,*], Youcai Zhu [a,b], Xueyu Du [a,b], Chaoliang Yao [c], Ying Ma [c], Jungang Zhao [a,b]

[a] College of Environmental Science and Engineering, Hunan University, Changsha 410082, PR China
[b] Key Laboratory of Environmental Biology and Pollution Control (Hunan University), Ministry of Education, Changsha 410082, PR China
[c] Yonker Environmental Protection Co., Ltd, Changsha 410330, PR China

ARTICLE INFO

Keywords:
BTEX
Material
Operating parameter
Mechanism
Practical application

ABSTRACT

BTEX with benzene ring and different groups (methyl and ethyl) have aroused enormous concern due to their wide sources and large contribution to photochemical reactions and ozone pollution. This paper systematically reviewed the photodegradation of BTEX including materials, operating parameters, and reaction mechanisms. The photocatalytic materials including monadic or binary metal oxides, hydroxides, and metal-free materials were broadened the optical absorption range and enhanced the absorption capacity by modifying, thus greatly improving the photocatalytic performance. The most effective strategy is forming the heterojunction with built-in fields, which enhances the light absorption capacity and leads lower recombination rate of photocarrier to generate more active oxygen species. The parameters of operating mode, initial concentration, flow rate, temperature, relative humidity and light play important roles in photocatalytic degradation of BTEX. Furthermore, this work highlights that the process of photo-oxidizing BTEX overwhelmingly follows the Langmuir-Hinshelwood model. The mechanisms including adsorption and surface reaction are described using the density functional theory calculations. The review reveals that BTEX are oxidized to the aldehyde and organic acids and opened the ring by active species, eventually mineralized to CO_2 and H_2O. Moreover, the different degradation pathways of BTEX are studied with the differences of position and number of methyl and ethyl groups. The technique combination is mostly used in the removal of BTEX due to complex working conditions in practical application. The challenge of catalyst inactivation can be regenerated by heating and UV cleaning.

1. Introduction

Recent decades have seen a growing tendency in the emissions of volatile organic compounds (VOCs), which has caused a series of air pollutions for their mobility and instability [1]. Anthropogenic VOCs, especially various industrial emissions [2], are precursors of ozone and photochemical smog, which are harmful to the environment and human health due to their toxicity, such as carcinogenicity, mutagenicity, and teratogenicity [3–6]. The vast majority of emitted VOCs consist of alkanes, alkenes, alkynes, aromatics, alcohols, aldehydes, ketones, esters, and halocarbons. Aromatics are recognized as high pollutants due to their large contribution to photochemical reactions and ozone pollution. Aromatic compounds (BTEX, benzene, toluene, ethylbenzene, and xylene), have a wide range of sources, such as automobile exhaust and organic solvents in building decoration materials, which have attracted great public attention [7]. BETX with different structures with benzene ring contribute to the majority of the total industrial emissions, which facilitate research and comparison. It is greatly worth noting the promising technologies for removing the aromatic compounds to protect the environment and human beings.

Over the past few decades, there are numerous abatement technologies to degrade BTEX, including absorption [8], adsorption [9], membrane separation [10], photocatalytic oxidation [11], catalytic oxidation [12], plasma destruction [13], and biological oxidation [14], etc. Among them, photocatalytic technology has gained increasing attention due to the highly efficient, low-energy, and harmlessness, which has broad application prospects in many fields [15,16]. At the background of conventional energy crisis, photocatalytic technology become the hot spot. Photocatalytic materials convert light energy into chemical energy under ultraviolet or visible light, and promote the

* Corresponding author at: College of Environmental Science and Engineering, Hunan University, Changsha 410082, PR China.
E-mail address: ctli@hnu.edu.cn (C. Li).

https://doi.org/10.1016/j.cej.2022.140461
Received 22 September 2021; Received in revised form 9 November 2022; Accepted 15 November 2022
Available online 17 November 2022

synthesis or decomposition of organic materials [17]. When the light energy is equal or exceeds to the bandgap energy of the semiconductor material, the electrons are excited from the valence band (VB) to the conduction band (CB) to form photo-generated carriers (electron-hole pairs), in which valence band holes are strong oxidants, while conduction band electrons are strong reductants [18,19]. Photogenerated electron-hole pairs can react with O_2 or H_2O adsorbed on the catalyst surface to produce superoxide radicals or hydroxyl radicals. These strongly active radicals can oxidize BTEX to mineralize to CO_2 and H_2O eventually [20].

Recently, some reviews on photocatalytic oxidation of VOCs have been published. The work of Shayegan's group has focused on the strategies for improving TiO_2 photocatalyst activities in VOCs degradation [21]. Vikrant *et al.* [22] spotlighted on the photocatalytic systems for benzene removal including the continuous mode and the batch mode. Zou *et al.* [23] summarized recent investigations on the integration of adsorption and photocatalytic degradation of VOCs using carbon-based nanocomposites. Besides, the key challenges for photocatalytic air purification to improving the applicability, including visible light utilization and catalyst deactivation have also been reported by Weon's group [24]. Nevertheless, to the best of our knowledge, little attention has been paid on the systematical review of the photocatalytic degradation of BTEX focusing on the mechanism of photocatalysis and discussing the practical application of BTEX photodegradation technology. In this review, we provide a detailed summary on the recent advances for BTEX removal using photocatalytic technologies. BTEX, as typical VOCs with special structure, can be systematically studied to understand the photocatalytic mechanism deeply and improve the practical application. Firstly, it provides an overview of photocatalytic materials including titanium dioxide, carbon nitride, zinc oxide and Bi-based photocatalyst, which have been mostly applied in BTEX removal. In addition, the operating parameters had a profound impact on the removal efficiency of BTEX. Furthermore, the kinetic model and mechanisms of photocatalytic decomposition of BTEX are described in detail. Finally, this article discusses the practical applications to combine other technologies with photocatalytic technology about the VOCs photodegradation and suggests some methods to rebirth the deactivated catalysts, which greatly improves the practical application of photocatalytic technology.

2. Materials for BTEX photocatalysis

2.1. TiO_2-based photocatalysts

Considering the economic and environmental benefits, TiO_2 is vigorously applied to the field of photocatalysis attributing to its excellent catalytic performance, stable chemical performance, safety, non-toxicity, and long service life [25,26]. In general, there are three crystal structures of TiO_2 in nature: rutile (Eg = 3.02 eV), anatase (Eg = 3.2 eV), and brookite (Eg = 3.14 eV). Among them, anatase TiO_2 has the best catalytic activity [27]. However, the application of TiO_2 is astricted by the large energy band gap, leading to only 4 % of the solar light utilization rate [24,28]. Besides, the development of TiO_2 is also hindered by the high rate of charge carrier recombination and insensitivity to visible light in photocatalysis (Fig. 1a). Accordingly, multifarious strategies have been developed vigorously, which include doping with metals and non-metals elements, and coupling with some semiconductors. The modified TiO_2 catalysts obtained by different methods exhibited better performance for photodegradation of BTEX, which listed in the Table 1.

2.1.1. Doping with metals

Noble metals play a major role in various organic conversions. Noble metal modified TiO_2 can greatly accelerate the separation of photo-generated electron-hole pairs significantly improving the photocatalytic activity [56,57]. Noble metals can promote the absorption of TiO_2 in visible light [58]. However, the use of noble metals for catalysis is greatly limited by their price. Non-noble metals (Mn, Fe, Cu, Ce, etc.) are often used as substitutes for modified TiO_2 due to their low price and wide source [59–61]. Non-noble metals can also narrow the band gap of

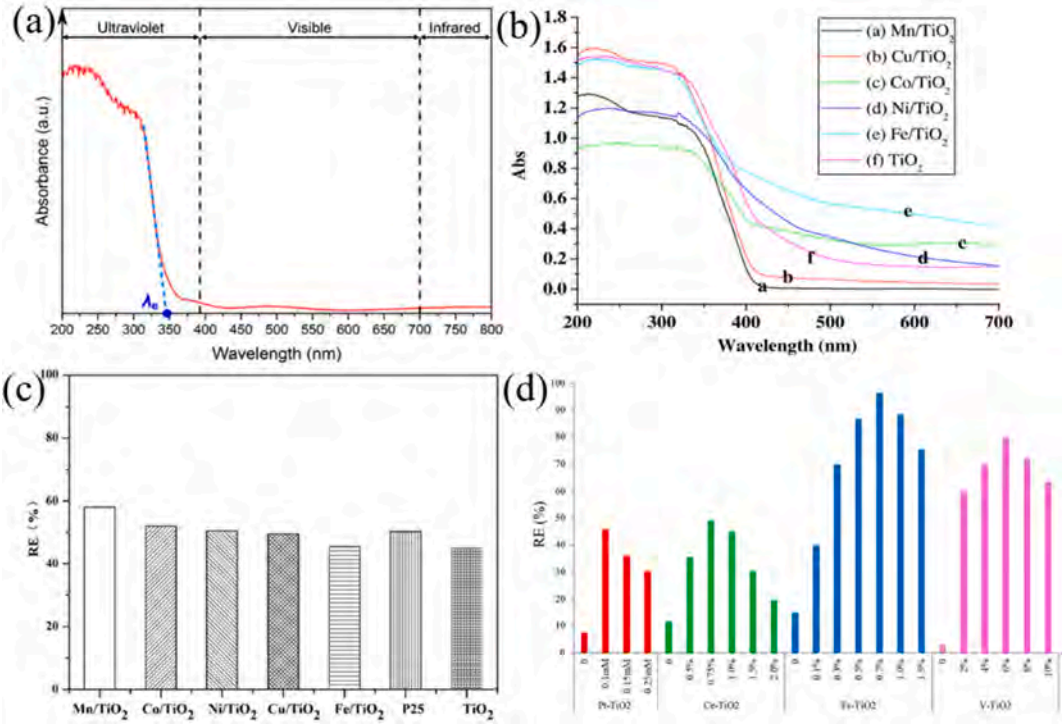

Fig. 1. (a) UV–vis diffuse reflectance spectra of TiO_2 thin film on glass [16]. (b) UV–vis diffuse reflection spectra of TiO_2 modified with non-noble metals [51]. (c) The removal efficiency (RE) of gaseous benzene on TiO_2 modified with various base metals [51]. (d) The RE of gaseous toluene on TiO_2 modified with different dopants metals [52–55].

Table 1
The photodegradation of BTEX using TiO_2-based photocatalysts.

Photocatalyst	Method	Light	BETX	Concentration	RE[a](%)	Reference
P25	wet impregnation	UV	benzene	2 ppm	20	[29]
			toluene	2 ppm	15	
			ethylbenzene	2 ppm	50	
			xylene	2 ppm	82	
Pt-P25	wet impregnation	UV	benzene	2 ppm	7	
			toluene	2 ppm	31	
			ethylbenzene	2 ppm	81	
			xylene	2 ppm	72	
Fe-P25	wet impregnation	UV	benzene	2 ppm	12	
			toluene	2 ppm	19	
			ethylbenzene	2 ppm	74	
			xylene	2 ppm	81	
Ce-P25	wet impregnation	UV	benzene	2 ppm	80	
			toluene	2 ppm	26	
			ethylbenzene	2 ppm	85	
			xylene	2 ppm	78	
V-TiO_2	solvothermal	visible	benzene	1000–1200 ppm	30	[30]
			toluene		68	
			ethylbenzene		76	
			xylene		83	
Fe-TiO_2	sol–gel	visible	benzene	0.1 ppm	3	[31]
			toluene	0.1 ppm	32	
			ethylbenzene	0.1 ppm	51	
			xylene	0.1 ppm	72	
N-TiO_2	sol–gel	UV	ethylbenzene	1000 ppm	20	[32]
N-TiO_2	sol–gel	visible	ethylbenzene	1000 ppm	13.5	[32]
N-TiO_2	sol–gel	visible	toluene	–	45	[33]
N-TiO_2	calcination	visible	benzene	–	72	[34]
CQDs/TiO_2	impregnation	UV/visible	o-xylene	50 ppm	87	[35]
C-TiO_2	sol-gel	UV	toluene	100 ppm	94	[36]
S-TiO_2-AS	sol-gel	visible	benzene	1 ppm	34	[37]
S-TiO_2-AS	sol-gel	visible	toluene	1 ppm	78	[37]
S-TiO_2-AS	sol-gel	visible	ethylbenzene	1 ppm	91	[37]
S-TiO_2-AS	sol-gel	visible	xylene	1 ppm	94	[37]
F-TiO_2	hydrothermal	UV	toluene	30 ppm	80	[38]
MnO_2/TiO_2	hydrothermal	VUV	toluene	30 ppm	96	[39]
Fe_2O_3/TiO_2	impregnation	fluorescent	o-xylene	50 ppm	91	[40]
CuO/TiO_2	impregnation	UV + Vis	o-xylene	60 ppm	35.67	[41]
CuO/TiO_2	impregnation	UV + Vis	m-xylene	60 ppm	34.48	[41]
CuO/TiO_2	impregnation	UV + Vis	p-xylene	60 ppm	30.38	[41]
WO_3/TiO_2	hydrothermal	visible	toluene	368 mg/m^3	85.3	[42]
WO_3/TiO_2	electrochemical	visible	toluene	200 ppm	90	[43]
ZnO/P25	impregnation	UV	toluene	500 ppm	~100	[44]
TiO_2-CeO_2	sol–gel	UV	toluene	10 ppm	96	[45]
MoS_2/TiO_2	hydrothermal	Visible	toluene	50 ppm	56	[46]
CuS/TiO_2	SILAR	solar light	toluene	4215 ppm	40	[47]
CdS/TiO_2	SILAR	solar light	toluene	4215 ppm	50	[47]
CdS/TiO_2	hybridization	visible	benzene	20 μg/mL	95	[48]
g-C_3N_4/TiO_2	impregnation	UV	toluene	200 ppm	67	[49]
$LaVO_4$/TiO_2	sol–gel	visible	benzene	250 ppm	70	[50]

[a] : The removal efficiency is defined as RE.

TiO_2 and strengthen the response of TiO_2 to the visible region, as shown in Fig. 1b. Metal ions, such as $Fe^{3+}$and Er^{3+}, dispersed in TiO_2 lattice break up the original lattice structure, forming lattice defects and shallow potential well [62,63]. The shallow potential well promotes the photocatalytic activity of the catalyst, which can prevent electron hole recombination. The TiO_2 modified with different metals has exhibited different degradation efficiencies (Fig. 1c). The mono-modified (Pt, Cu, Ag) TiO_2 photocatalysts were prepared by chemical reduction method [64]. The absorption spectra of obtained photocatalysts indicated that the visible light absorption of all metal-modified photocatalysts was significantly enhanced compared to the pure titanium (IV) oxide. The types and amounts of doped metal are the decisive parameters of TiO_2 photocatalysis. Huang *et al.* [51] studied the catalytic oxidation of benzene on TiO_2 modified with base metals (Mn, Co, Cu, Ni, and Fe). The presence of base metals probably promoted the transformation from anatase phase to rutile one. The shifts of the absorption on various metals were different, so did the removal efficiency of benzene (Fig. 1c). Fig. 1d shows the photodegradation of toluene by metal-TiO_2 with different loadings. With the amount of doped metal increasing, the degradation efficiency of toluene initially increased and subsequently decreased for all catalysts. If a certain amount of metal dopant is maintained, dopants trap electrons generated by the photoelectricity and separate charge carriers, like an electron acceptor [54,65]. However, in high dopant concentration, dopants may act as a recombination center preventing hole formation and even distort the catalyst crystallinity, which reduces the photocatalytic reactivity greatly [62,64]. As we can see in the Table 1, P25 catalysts modified with different metals were used to degrade BTEX in the gas phase under UV irradiation, and Ce-P25 exhibited better performance for BTEX degradation [29]. Additionally, the oxidation rate of the BTEX (R_A, ppmv/min), the adsorption constant (K_A, $ppmv^{-1}$), and the rate constant (k_R, ppmv/min) were calculated using the experimental data. The K_A about ethylbenzene and xylene were substantially higher than those of benzene and toluene, which indicated that ethylbenzene and xylene were more easily adsorbed than benzene and toluene. The k_R about benzene and ethylbenzene which data obtained over Ce-P25 were higher than those about toluene and

xylene which data obtained over Ce-P25 and those about BTEX which data obtained over P25 and Fe-P25, revealing the stronger photodegradation of benzene and ethylbenzene using Ce-P25.

2.1.2. Doping with non-metals

The drawback of doping metals is easy to photo-corrode during the photocatalytic process. Non-metallic elements have the advantages of wide source of raw materials, low prices, and resistance to corrosion. As a result, the preparation of TiO_2 photocatalyst by using non-metals is a feasible way to reduce the band gap and enhance the response of visible light. Carbon (C), nitrogen (N), fluorine (F) and sulfur (S) are common TiO_2 non-metallic dopants used to remove VOCs (Fig. 2a) [66,67]. Doping carbon can not only increase the crystallinity of TiO_2, but also make the absorption wavelength red-shift [68]. Mahmood' group also expounded that the carbon quantum dots (CQDs) notably improved the adsorption capability of TiO_2, attributing to the hexagonal ring structures in CQDs [35]. Nitrogen has a low ionization energy, good stability. Doping nitrogen also can reduce the band gap of TiO_2. Fig. 2b shows that the different structures of N-TiO_2, including substitutional and interstitial. Li's group investigated the degradation of benzene on N—H—TiO_2 photocatalyst [69]. It was found that the new doping states above the VB edge and defect states appeared with N—H—codoping (Fig. 2c), which increased the surface reactive sites and reduced the recombination of charge carriers, thus improving the photocatalytic reaction. Valentin *et al.* [70] found that TiO_2 doped with carbon or nitrogen would produce alternative and interstitial crystal structures. X-ray photoelectron spectroscopy (XPS) analysis revealed that the peak at 399.6 eV was regarded as the substitutional N and the peak at 401.6 eV was attributed to the interstitial N [71]. The atomic radius of carbon and nitrogen is similar to that of the oxygen atom, and the electronegativity is weaker than oxygen. Therefore, Carbon and nitrogen may supersede oxygen in the TiO_2 lattice. On the other hand, since carbon and nitrogen atoms are highly small, they may diffuse through the lattice voids and then combine with the lattice atoms. Conversely, fluorine has a higher electronegativity than oxygen. And the F 2p states are under the bottom of the O 2p VB. The introduction of fluorine may bring about the appearance of the impurity states in the band gap of TiO_2 and formation of Ti^{3+} states (Fig. 2a). Ti^{3+} states can effectively capture photo-generated electrons, which can suppress the recombination of electron-hole pairs and improve its photocatalytic performance [38]. In term of S with various valence states, the mixing of the 3p orbit of S and the valence band can reduce the forbidden bandwidth. Doping S can also facilitate the separation of electron-hole pairs [72]. S-TiO_2 films immobilized on aluminum sheets exhibited excellent performance for decomposing the BTEX under visible light irradiation [37].

2.1.3. Doping with semiconductors

The composites of semiconductors are catalysts obtained by compounding different semiconductors with titanium dioxide nanomaterials by using the coupling effect between nanoparticles. Composites outperform single semiconductors because the difference of chemical potential between semiconductors causes band bending at the interface of junction. A built-in field is generated by the band bending, resulting in a spatial separation of the electrons and holes on different sides of heterojunction. There are several semiconductors with different band edges, and semiconductor compounding includes three methods (Fig. 3a). The first is to connect with narrow-bandgap semiconductors (CdS, C_3N_4, etc.). For instance, combined with CuS and CdS, the composites of CuS-CdS/TiO_2 generated a stepwise energy level structure because the CB and VB edges of the three materials both increased in the order of TiO_2 < CdS < CuS, thereby obtaining a higher driving force for the electron injection at the interfaces and highly suppressing the recombination of electron-hole pairs [47]. The second is to use wider band metal oxides (ZnO, SnO_2, etc.) to suppress electron recombination. The heterojunction was formed between TiO_2 and SnO_2 (Eg = 3.8 eV), and the electrons generated from TiO_2 were shifted to SnO_2 [74]. The charge-transfer process caused a better performance. The third is to combine with p-type semiconductor (CuO, etc.) on *n*-type TiO_2 semiconductor to improve the photocatalytic efficiency. The energy band structure and density of TiO_2 and CuO-TiO_2 composites were calculated

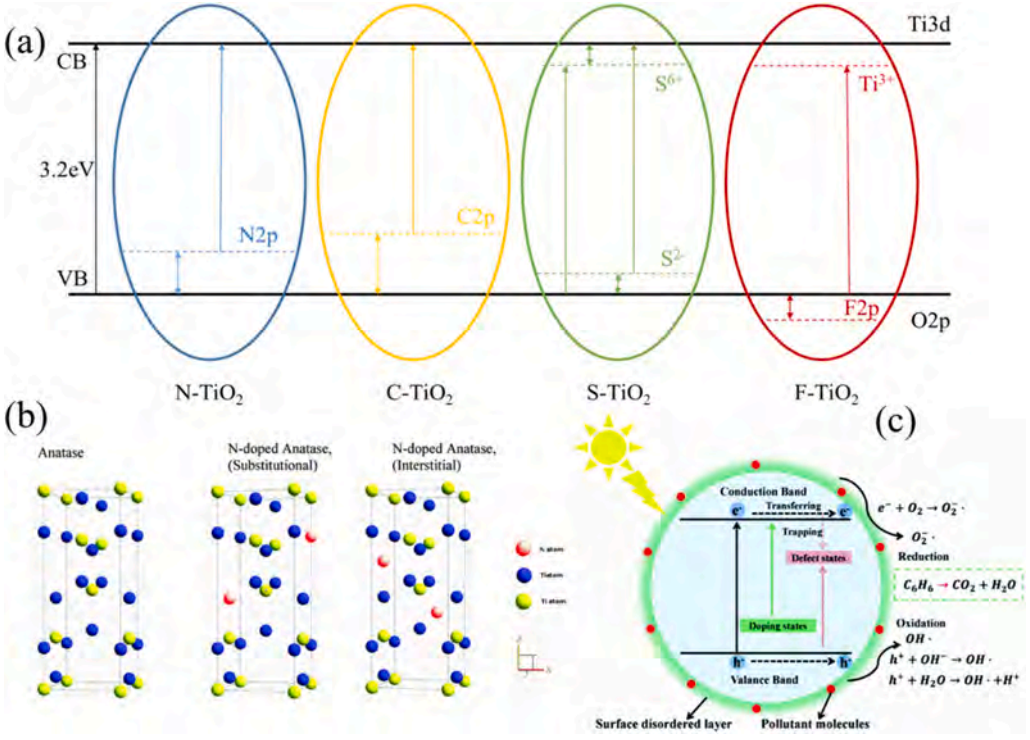

Fig. 2. (a) Schematic energy level of TiO_2 doped with non-metals. (b) The structures of the three different forms of *N*-dopped Anatase [73]. (c) Schematic diagram of energy states and photocatalytic reaction paths on N—H—TiO_2 nanoparticles [69].

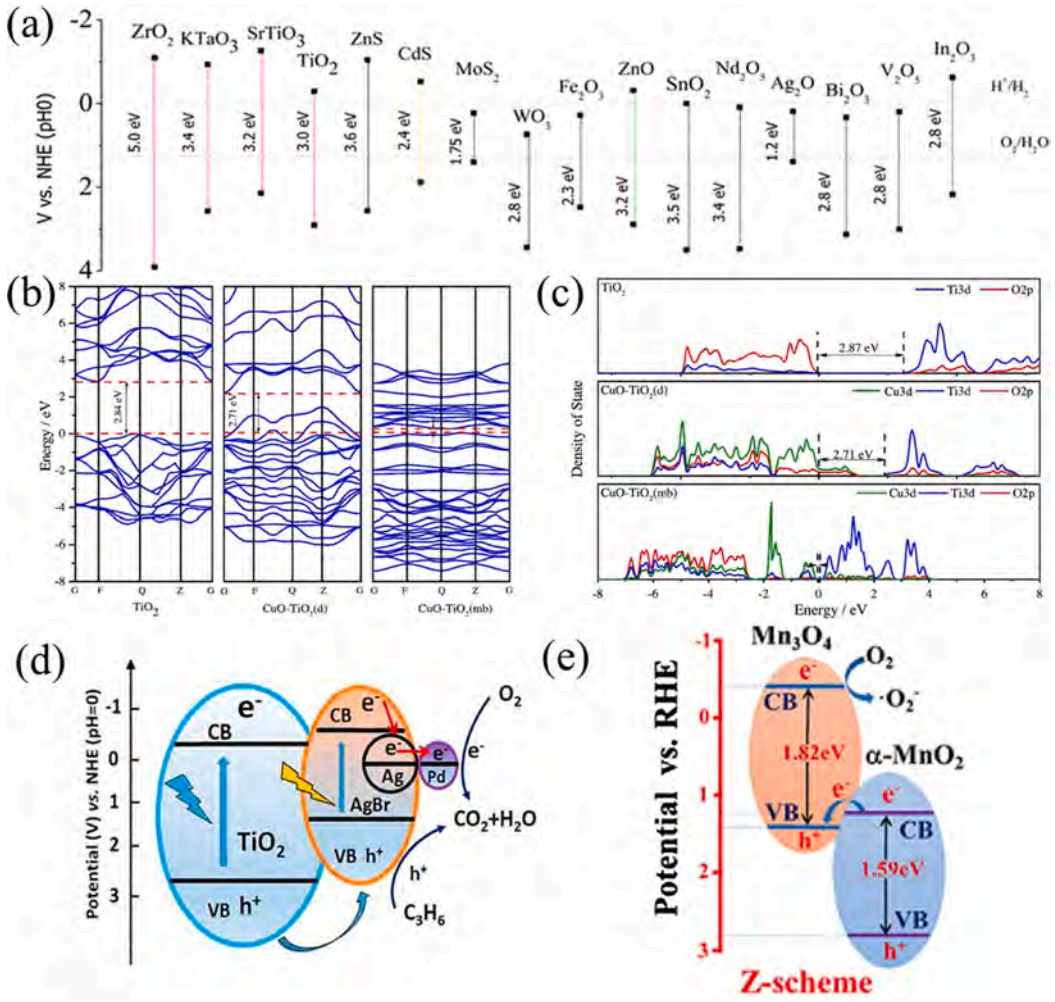

Fig. 3. (a) Band edge position of diverse semiconductors, using the normal hydrogen electrode (NHE) as a reference [75]. (b) Band structure and (c) density of state of TiO_2 and CuO-TiO_2 composites [41]. (d) The photocatalytic mechanism of Pd-Ag/AgBr/ TiO_2 hierarchical nanostructure [76]. (e) Z-scheme charge-transfer mechanism for the α-MnO_2/Mn_3O_4 system [77].

by the density functional theory (DFT) [41]. As shown in Fig. 3b, the indirect band gap of TiO_2 was 2.84 eV initially, and the band gap reduced to 2.71 eV and even to 0.14 eV with the introduction of CuO. Fig. 3c displays that the orbit of Cu 3d and O 2p participated in the hybridization and generated more impure states, thereby leading to a lower band gap.

Sulfides such as MoS_2 (1.75 eV), CuS (2.00 eV), and CdS (2.40 eV) are common narrow-bandgap semiconductors. The CuS/TiO_2 and CdS/TiO_2 photocatalysts were successfully prepared via simple successive ionic layer adsorption and reaction (SILAR) method used for removal of toluene [47]. The absorption edge of TiO_2 had a red shift on account of the loading of CuS or CdS composition, resulting in a better visible light response ability. The PL emission spectra elucidated that the order of the recombination of free carriers was as follows CuS/TiO_2 nanobelts < CdS/TiO_2 nanobelts < TiO_2 nanobelts. In addition, MoS_2 could enhance the photocatalytic activity with the exposed sulfur atoms behaving as active sites. Hence, MoS_2/TiO_2 composites displayed a predominant degradation efficiency of gaseous toluene, prepared by a facile hydrothermal reaction [46]. A series of TiO_2/MnO_2 nanosheets with different percentage of Mn were characterized by UV–vis diffuse reflectance spectra (DRS). The absorption range of samples was extended from 410 nm to near infrared light. Besides that, as the amount of MnO_2 increased, the light absorption intensity of TiO_2/MnO_2 nanosheets in visible light regions increased [39]. Nevertheless, ZnO/P25 composites prepared by an incipient wetness impregnation method degraded the gas toluene exposing to the UV lamp [44]. With the increase of ZnO content, the light absorption intensity increased at the initial stage and then decreased, and the toluene conversion rate also increased firstly and then decreased. There was a special charge transfer mechanism of the bimetallic Pd-Ag co-catalyst on AgBr/TiO_2 composites in Fig. 3d [76]. The AgBr/TiO_2 heterostructure was a type-II semiconductor, which enhanced the charge separation and the visible light utilization. In addition, the existence of Ag and Pd improved the charge transfer, thereby greatly promoting the photocatalytic process.

2.2. *Non-TiO_2 photocatalysts*

The major types of non-TiO_2 photocatalysts used on BTEX removal are monadic or binary metal oxides, hydroxides, Bismuth-based materials, and metal-free materials. Those materials with different bandgap obtained different methods were listed in Table 2, which were used in the photodegradation of BTEX.

2.2.1. *Metal-oxide-based semiconductor*

There are many valence states for manganese. Different valence states of manganese oxides can form heterojunctions, which can effectively prevent the recombination of photogenerated electrons and holes, thus improving the photocatalytic activity. The hierarchical porous α-MnO_2/Mn_3O_4 nanostructures with multiple interfaces were successfully designed and synthesized [77]. As shown in the Fig. 3e, the direct

Table 2
The photodegradation of BTEX using non-TiO_2 photocatalysts.

Photocatalyst	Light	BETX	Concentration	RE (%)	Reference
ZnO	sunlight	benzene	50 ppm	57	[78]
ZnO	sunlight	toluene	50 ppm	67	[79]
ND-ZnO	UV	toluene	50 ppm	100	[80]
Si-GO/ZnO	UV	toluene	100 ppm	76.18	[81]
Silica-GO/ZnO	UV	benzene	50 mg/m^3	87.20	[82]
ZnO-13X zeolite	UV	benzene	5 ppm	98.4	[83]
ZnO-AC	UV	benzene	5 ppm	99.0	[83]
Ɛ-MnO_2/C	visible	toluene	56 mmol/L	87.34	[84]
α-MnO_2/Mn_3O_4	Xenon lamp	toluene	300 ppm	>90	[77]
M−CeO_2	VUV	toluene	30 ppm	82.0	[85]
N-CeO_2	VUV	toluene	30 ppm	87.8	[85]
T-CeO_2	VUV	toluene	30 ppm	87.9	[85]
WO_3	Xenon lamp	toluene	2800 mg/m^3	73.8	[86]
ZnCr–LDHs	visible	o–xylene	175 mg/m^3	40.9	[87]
Au/ZnCr–LDHs	visible	o–xylene	175 mg/m^3	83.6	[87]
Au/ZnCr–LDHs	visible	m–xylene	175 mg/m^3	79.7	[87]
Au/ZnCr–LDHs	visible	p–xylene	175 mg/m^3	77.8	[87]
Au/ZnCr–LDHs	visible	benzene	175 mg/m^3	97.7	[87]
Au/ZnCr–LDHs	visible	toluene	175 mg/m^3	91.4	[87]
$MgSn(OH)_6$	UV	benzene	250 ppm	~70	[88]
$ZnSn(OH)_6$	UV	benzene	250 ppm	88	[88]
$CaTiO_3$	UV	toluene	50 mg/L	~65	[89]
Eu^{3+}-$CaTiO_3$	UV	toluene	50 mg/L	~80	[89]
Pt/$SrTiO_3$	visible	toluene	700 ppm	85	[90]
$BaZrO_3$	visible	toluene	–	~34	[91]
$SrZrO_3$	visible	toluene	–	~23	[91]
$LaFeO_3$	UV–vis	p-xylene	19 mg/L	35.8	[92]
$LaMnO_3$	UV–vis	p-xylene	19 mg/L	37.6	[92]
$LaCoO_3$	UV–vis	p-xylene	19 mg/L	26.1	[92]
$LaFeO_3$	visible	benzene	–	85	[93]
$KTaO_3$	visible	toluene	150 ppm	47	[94]
$KTaO_3$	visible	toluene	200 ppm	13.11	[95]
Pt/Er-$KTaO_3$	visible	toluene	200 ppm	30.92	[95]
Rh/Pr-$KTaO_3$	visible	toluene	200 ppm	34.73	[95]
$KTaO_3$	visible	toluene	200 ppm	17.13	[96]
Au-$KTaO_3$	visible	toluene	200 ppm	29.29	[96]
Ag-$KTaO_3$	visible	toluene	200 ppm	30.43	[96]
Pt-$KTaO_3$	visible	toluene	200 ppm	36.42	[96]
Pd-$KTaO_3$	visible	toluene	200 ppm	33.34	[96]
Rh-$KTaO_3$	visible	toluene	200 ppm	41.98	[96]
Ru-$KTaO_3$	visible	toluene	200 ppm	25.68	[96]
$ZnFe_2O_4$	UV	toluene	900 ppm	~60	[97]
$ZnFe_2O_4$	visible	toluene	900 ppm	~34	[97]
$CaFe_2O_4$	visible	toluene	–	76	[98]
$ZnGa_2O_4$	UV	benzene	220 ppm	20	[99]
$ZnGa_2O_4$	UV	toluene	180 ppm	26	[99]
$ZnGa_2O_4$	UV	ethylbenzene	190 ppm	30	[99]
$ZnCo_2O_4$	UV	toluene	–	78	[100]
Bi_2WO_6	visible	toluene	250 ppm	80.6	[101]
Pt/Bi_2WO_6	visible	toluene	250 ppm	>90	[101]
Bi_2WO_6	visible	toluene	350 mg/m^3	45.9	[102]
CQDs/Bi_2WO_6	visible	toluene	350 mg/m^3	96.9	[102]
Bi_2WO_6	visible	benzene	100 ppm	~38	[103]
BiOCl/ Bi_2WO_6	visible	benzene	100 ppm	~20	[103]
BiOCl	visible	benzene	100 ppm	~12	[103]
BiOCl	UV	toluene	50 ppm	52.5	[104]
BiVO4	visible	toluene	25 ppm	~30	[105]
$BiO_{1.2}I_{0.6}$	Xenon lamp	toluene	2800 mg/m^3	82.3	[86]
$BiO_{1.2}I_{0.6}$ /WO_3	Xenon lamp	toluene	2800 mg/m^3	>95	[86]
$(BiO)_2CO_3$	visible	toluene	1200 ppm	~22.5	[106]

Z-scheme heterojunction mechanism indicated that the photogenerated electrons in the CB of α-MnO_2 migrated to the VB of Mn_3O_4 and recombined with holes, leading to effective spatial charge separation. The accumulated electrons in the CB of Mn_3O_4 were captured by the absorbed oxygen on the surface to generate $\bullet O_2^-$ radicals that participated in photocatalysis. MnO_2 with a narrow band gap, has a wide range of absorption under sunlight. Zhou *et al.* [84] discovered a 3D hierarchical ε-MnO_2 pasted with carbon. The C-coated ε-MnO_2 could expand the photo-response from UV to visible light region, thus generating more electron-hole pairs and exhibiting unexceptionable performance for removing toluene.

ZnO is a promising semiconductor material which has a broad band gap width (3.2 eV, Fig. 3a) and a large excitation binding energy (60 meV) [107]. Furthermore, the absorption efficiency of ZnO in the solar spectrum is higher than TiO_2. ZnO is considered an attractive alternative to titanium dioxide on account of their similar chemical-physical characteristics. ZnO also has the advantages of stable chemical properties, abundant appearance, biological safety and low cost. The catalytic degradation of benzene and toluene by ZnO coated on glass plates was studied under simulated sunlight, which had a relatively superior efficiency [78,79]. Like TiO_2, doping ZnO with metal or nonmetal displayed a highly efficient degradation of BTEX, as seen in Table 2. The noble

metal can effectively capture electrons as an electron acceptor [108]. Modified with Ag, ZnO had excellent activity for benzene removal on account of the strong separation of photo-generated electrons and holes [108]. The Pd was introduced into the ZnO superstructures doped by carbon using the sol- immobilization process, which had better photo-thermal catalytic performance towards benzene oxidation [109]. The existence of defects and oxygen vacancies caused by doping C, promoted the oxygen species transportability and enhanced the catalytic activity as active sites [110]. In addition, some carbon materials are also commonly used to improve photocatalytic performance. Graphene can prevent the recombination of charges during electron transport, thereby improving the photocatalytic activity of ZnO. On the other hand, the high specific surface area and high adsorption rate of graphene enhance the contact between pollutants and ZnO, which promotes pollutants degradation [81,82]. However, the photocorrosion of ZnO is a common and serious phenomenon that often occurs in the long-term photo-catalysis process, which greatly hinders its further application. Liu *et al.* [80] successfully developed a strategy to suppress photocorrosion of ZnO with introducing the nanodiamonds (ND). The modification of ND not only effectively inhibited the photocorrosion to prolong the working life, but also greatly enhanced the photocatalytic ability. With the decoration of ND, free electrons of ND could transfer to ZnO to form a built-in electric field, and the photo-generated h^+ and formed O_2^- participated in the degradation of toluene (Fig. 4a).

CeO_2 is a rare-earth oxide that has a broad direct band gap width (3.2 eV) and light absorption edge (388 nm) [16]. CeO_2 has excellent photocorrosion resistance, and has excellent ultraviolet light absorption capacity. However, it is more important that the active surface sites can arise by switching readily between Ce^{4+} and Ce^{3+}, giving rise to the formation or destruction of associated oxygen vacancy easily. And the redox properties of Ce^{4+}/Ce^{3+} pairs might lead to the motivation of hydroxyl radical generation [111]. Also, there are some correlations between the activity and structure of CeO_2. Mesoporous microcuboid CeO_2 (M−CeO_2), CeO_2 nanorods (N-CeO_2), and CeO_2 with tunable porosity (T-CeO_2) were formed and applied for the removal of toluene under VUV irradiation [85]. The UV–vis DRS demonstrated that three

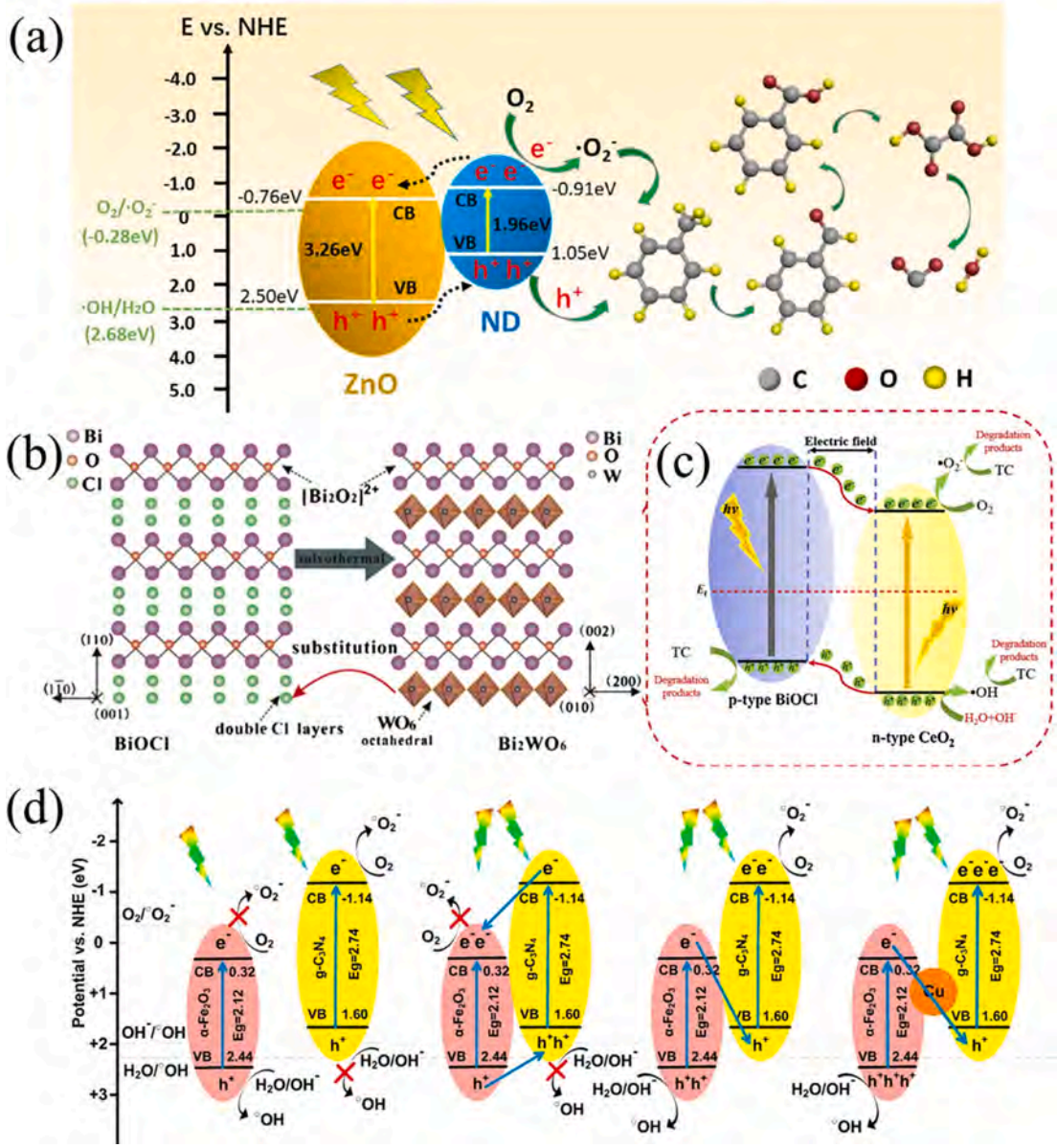

Fig. 4. (a) The proposed mechanism for photocatalytic degradation of toluene upon nanodiamond-decorated ZnO [80]. (b) The structures of BiOCl and Bi_2WO_6 in the Bi-W-Cl-O solvothermal system [103]. (c) The novel hollow BiOCl@CeO_2 heterostructure [114]. (d) The proposed heterojunction mechanisms between α-Fe_2O_3 and g-C_3N_4 [115].

samples had stronger absorbance in the UV region and weaker absorbance in the visible region, relatively. The results of VUV-photocatalytic oxidation indicated that N-CeO_2 and T-CeO_2 exhibited higher removal efficiency of toluene. Pd-Ag@CeO_2 which had a core–shell structure significantly improved the light adsorption and charge separation in the visible region [112]. The synergistic effect of Pd and Ag weakened the Ce-O bond and produced a high concentration of lattice defects, which further promoted the transformation of lattice oxygen and adsorbed oxygen.

WO_3 has a broad direct band gap width (2.8 eV, Fig. 3a). And WO_3 can more effectively utilize visible light, which accounts for nearly half of the solar radiation energy. Wang *et al.* [86] found that WO_3 exhibited remarkable catalytic performance for photocatalytic toluene. However, pure WO_3 is difficult to maintain stable photocatalytic performance, thanks to defects such as easy photocorrosion and low utilization rate of visible light. Hence, WO_3 is often doped with metals or coupled with other semiconductors to improve its photocatalytic performance [43,113].

2.2.2. Hydroxide photocatalysts

Most degradation reactions are mediated by hydroxyl radicals (•OH), and the formation of hydroxyl radicals can be effectively promoted by surfaces with high hydroxyl density. It is necessary to generate OH radicals in the process of photocatalytic oxidation, so hydroxides are also often used as photocatalysts to degrade VOCs. A series of $MSn(OH)_6$ (M = Co, Cu, Fe, Mg, Mn, Zn) was synthesized and exhibited obvious visible absorptions [88]. Only $MgSn(OH)_6$ and $ZnSn(OH)_6$ displayed a predominant and stable activity for the destruction of benzene. In these samples, the hydroxyl structure gave them high performance, promoted the formation of active radicals (•OH and $\bullet O_2^-$), and inhibited the deposition of stable by-products. According to the research, ZnCr-LDHs (Layered Double Hydroxides) with narrow band bap had considerable reactivity for photocatalytic reaction, which had a good deal of water molecules and hydroxyl ions [87]. The water molecules and hydroxyl ions were the key to the generation of OH radicals during photocatalytic oxidation. Above all, the active species experiments revealed that the major drive of photocatalytic reaction was the hole and hydroxide radicals for Au supported ZnCr-LDHs. This indicated that Au/ZnCr-LDHs exhibited higher photocatalytic activity.

2.2.3. Perovskite oxides

Perovskite (ABO_3) oxide has become one of the researches focuses in the field of photocatalysis due to its stable structure, narrow band gap, wide light absorption wavelength range, and high solar energy utilization rate. The $CaTiO_3$ perovskites were studied for photocatalytic degradation of toluene [89]. The adsorption edges of the $CaTiO_3$ perovskites shifted to a longer wavelength of ca. 400 nm. The perovskite $LaMO_3$, as a highly efficient photocatalyst rich in earth, has attracted great attention. This structure benefits from the possibility of replacing M. Different M not only results in controlling the band gap, but also ultimately controlling the energy arrangement of the surface, such as oxygen vacancies which can contribute to the higher photocatalytic activity. The perovskite-like oxides $LaBO_3$ (B = Fe, Co, and Mn) were prepared by sol–gel method which exhibited ascendant stability and activity for photodegradation of p-xylene under radiation of UV–vis light [92]. It indicated that the band gap energy (Eg) for perovskites $LaBO_3$ was about 1.87–2.2 eV, leading to absorption increasing in the visible region. Jamali *et al.* [93] found that $LaFeO_3$ nanoparticles had a narrow band gap energy (2.12 eV) and mesoporous structure, with high crystallinity. $KTaO_3$ was also commonly used as a photocatalyst with high photochemical stability and a relatively wide band gap of about 3.4 eV (Fig. 3a), resulting in that it can only be excited by UV. Krukowska *et al.* [95,96] studied that $KTaO_3$ decorated with mono or bimetallic nanoparticles had predominant Vis and UV–vis light activity for toluene removal in gas phase. Therefore, Metals are often doped in $KTaO_3$ for broadening light absorption to longer wavelengths.

2.2.4. Spinel oxides

Spinel-type complex oxide (AB_2O_4) has advantages of visible light response, stable structure, diverse composition, narrow band gap, etc. It can adjust its structure while maintaining the original configuration unchanged and improve the visible light absorption efficiency of the materials. Hence, spinel oxide is an ideal material for exploring new photocatalysts with large visible light absorption range and high quantum conversion efficiency, as illustrated in Table 2. Zhou *et al.* [100] established hollow porous zinc cobaltate ($Zn_xCo_{3-x}O_4$) nanocubes in order to heighten the photocatalytic performance of spinel oxides. Compared with traditional stoichiometric $ZnCo_2O_4$ nanoparticles, the $Zn_xCo_{3-x}O_4$ nanocubes had a higher specific surface area, stronger light absorption capacity in the range of 350–800 nm, and lower recombination rate of photogenerated electron-hole pair. And Fe-base spinel materials exhibit high catalytic stability on account of the framework structure of Fe-O octahedrons. Meanwhile, The Fe d-orbitals of AFe_2O_4 play a major role in the formation of narrow band gaps, which can broaden light absorption to longer wavelengths. Using spinel-type mesoporous nano-$ZnFe_2O_4$ (1.87 eV) as photocatalyst, toluene, a metabolite of VOCs pollutants, can be effectively removed under UV and visible light irradiation [97]. Yin *et al.* [98] had designed a novel hedgehog-like $CaFe_2O_4$ hollow-structured materials by a simple template-assisted method. The characterization results showed that this new structure could significantly improve the separation and transformation of photogenerated e^-/h^+ pairs.

2.2.5. Bismuth-based catalysts

Bismuth-based compounds have become a research hotspot in the field of non-TiO_2 photocatalyst development in recent years due to their special layered structure and appropriate band gap. From the perspective of its electronic structure, the hybridization of 6s orbital of Bi and 2p orbital of O causes its valence band to move up, which is conducive to the separation and migration of photo-generated e^--h^+ pairs during photocatalysis. Therefore, bismuth-based photocatalysts have good photocatalytic performance. As can be seen from the Table 2, Bismuth-based photocatalysts commonly used to catalyze VOCs include ternary metal oxides, bismuthate and bismuth oxyhalides.

A typical binary metal oxide Bi_2WO_6 has an orthorhombic Aurivillius-type structure composed of alternating bismuth oxide $[Bi_2O_2]^{2+}$ and octahedral $(WO_6)^{2-}$ (Fig. 4b). Due to the narrow band gap (2.5–2.8 eV), Bi_2WO_6 has strong absorption under visible light and favorable light stability. The Bi_2WO_6 composites modified with Pt have a high concentration of oxygen vacancies [101]. The oxygen vacancies below the CB might reduce the band gap of Bi_2WO_6 and facilitate the formation of $\bullet O_2^-$, accelerating the mineralization of gaseous toluene. And simultaneously, the deposition of Pt promoted the separation of photogenerated charge pairs. Liu *et al.* [102] introduced carbon quantum dots (CQDs) in Bi_2WO_6 to remove toluene under visible light, which makes the light absorption red-shifted and oxidizing ability enhanced. Furthermore, the CQDs/Bi_2WO_6 behaved high stability and reusability. And monoclinic $BiVO_4$ is another common catalyst with high activity. The estimated band gap of $BiVO_4$ is 2.17 eV giving rise to strong absorption of visible light [105].

Bismuth oxyhalides BiOX (X = F, Cl, Br, I) have outstanding optical and electrical properties, which are crystallized in a tetragonal matlockite structure. As shown in Fig. 4b, BiOCl is a layered semiconductor photocatalyst composed of $[Bi_2O_2]^{2+}$ layers and Cl^- alternately combined. BiOCl with a large band gap (3.4 eV) has high insensitivity to visible light [103]. Three stages including BiOCl, BiOCl/Bi_2WO_6 composites, and Bi_2WO_6 were prepared by changing the reaction conditions in the Bi-W-Cl-O system [103]. The UV–vis DRS spectra revealed that Bi_2WO_6 had a higher light efficiency than BiOCl. In addition, the photocatalytic efficiency of the three samples for benzene under visible light was arranged as Bi_2WO_6 > BiOCl/Bi_2WO_6 composites > BiOCl. Dong *et al.* [104] successfully constructed the surface oxygen vacancies (OVs) on the surface of BiOCl via the solvothermal-induced hot ethylene glycol

reduction. The introduction of OVs enhanced the adsorption and activation of O_2, H_2O and toluene molecules to generate more reactive free radicals with higher oxidation capacity. As we can see in Fig. 4c, a type-II heterostructure was formed between p-type BiOCl and *n*-type CeO_2, which established a new Fermi level balance leading to the alteration of energy band of two semiconductors [114]. The internal electric field was built by the transfer cycle of h^+/e^-, and promoted the separation of h^+/e^-, thus improving the photocatalytic performance. BiOI is an attractive semiconductor with a layered crystal structure and a suitable band gap. Nonetheless, the rapid recombination of charge and poor electrical conductivity lead to low photocatalytic efficiency, which hinders the practical application of BiOI. Herein, Wang *et al.* [86] synthesized a novel photocatalytic composite material of I-deficient $BiO_{1.2}I_{0.6}/WO_3$ by solvothermal method coupling with thermal decomposition. The introduction of iodine vacancy and WO_3 prominently strengthened the photocatalytic activity of BiOI.

$(BiO)_2CO_3$ is an orthogonal crystal structure in which $[Bi_2O_2]^{2+}$ layer and $[CO_3]^{2-}$ layer are alternately arranged. The pure $(BiO)_2CO_3$ can only absorb the UV light up to 370 nm, which can be assigned to the band gap of $(BiO)_2CO_3$ for 3.2 eV. To expand the light absorption of $(BiO)_2CO_3$, Duan *et al.* [106] successfully synthesized a ternary heterojunction $(BiO)_2CO_3$-CdS-CuS. It was found that the band gap of the $(BiO)_2CO_3$-CdS-CuS heterojunction was reduced to about 2.25 eV, which showed preeminent catalytic activity and stability for toluene degradation.

2.2.6. Graphitic carbon nitride

The simple graphitic carbon nitride (g-C_3N_4) with a suitable band gap is an ideal candidate material for a new generation of the visible light responsive photocatalyst. The g-C_3N_4 is a non-toxic, low-cost, metal-free, stable semiconductor made from readily available starting materials containing the most abundant elements (carbon and nitrogen). Zhao *et al.* [116] studied that the catalytic activity of pure g-C_3N_4 for benzene was weaker than that of TiO_2. The low specific surface area and high photocarrier recombination rate limited the application of g-C_3N_4. Therefore, g-C_3N_4 is often combined with other semiconductors to enhance its activity. The custom-designed $H_3PW_{12}O_{40}$/g-C_3N_4 film-coated optical fiber photoreactor was demonstrated for removal of aromatics including benzene, toluene and m-xylene under simulated sunlight [117]. The $H_3PW_{12}O_{40}$/g-C_3N_4 film exhibited remarkably higher photocatalytic activities which had better stability and recyclability. A novel α-Fe_2O_3/Cu/g-C_3N_4 nanocomposite successfully prepared by a simple and facile procedure showed excellent photocatalytic performance and stability for the removal of air ethylbenzene [115]. As shown in Fig. 4b, there were two probable mechanisms including type-II heterojunction and Z-scheme system. The type-II heterojunction mechanism can't produce ·OH and $\cdot O_2^-$ radicals due to the CB edge potential of α-Fe_2O_3 and the VB edge potential of g-C_3N_4. The Z-scheme mechanism was rational in which the fast combination happened between the CB-electrons of α-Fe_2O_3 and the VB-holes of g-C_3N_4. Furthermore, the introduction of Cu promoted the transformation and combination of weak charge carriers.

2.3. Summary

In conclusion, it is important for the photocatalytic materials to convert light energy into chemical energy in the photocatalytic degradation of BTEX, which could generate the electron-hole to form the active oxygen species. Although, semiconductors with a narrow band gap excites electrons to advance from the valence band to the conduction band with relatively low photon energy, the lifetime of photogenerated electron is too short. Through investigation, it is found that both TiO_2-based and non-TiO_2 photocatalytic materials exhibited different performance on BTEX removal. However, compared with semiconductor monomers or doping elements, heterojunction composites show excellent performance, so it is worth further study on forming the heterojunction using the semiconductors with different bandgap. There is a band bending at the interface of heterojunction owing to the difference of valance and conduction bands, and a built-in field might be formed. The built-in field could drive the electrons and holes to move in opposite directions, which lead lower recombination rate of photocarrier to generate more active oxygen species. Therefore, it is crucial to choose the semiconductors and design the heterojunction for photodegradation of BTEX.

3. The effect of operating parameters

3.1. Operation mode of photocatalytic system

The mode of operation plays a vital role in the photocatalytic system of gaseous BTEX, which may dramatically alter performance. Generally speaking, there are two modes of photocatalytic operation including continuous mode and batch mode. For continuous mode system, a certain concentration of gaseous BTEX continuously is carried out in reactor. Due to the limited exposure time and sustained high concentration, the continuous mode system exhibits lower performance at the same light source [31,41]. The continuous mode system is mostly used with the smaller footprint and larger handling capacity in large-scale industries [118]. On the contrary, the batch mode system includes a closed reactor. The target pollutants could interact with active species and be degraded deeply in the closed reactor, which exhibits higher performance [80,119]. The batch mode usually applies to some small-scale industries owing to its simple operation and maintenance [120].

3.2. Initial concentration and flow rate

Photocatalytic oxidation which is heterogeneous reaction generally includes three processes: adsorption, surface reaction, and desorption. For the surface reaction, active species oxidize a certain amount of BTEX into small molecules and even mineralize to H_2O and CO_2. On the one hand, increasing the concentration of BTEX drives the kinetics [97]. And a higher initial concentration could boost the probability of active substances or high-energy particles colliding with BTEX molecules [121]. On the other hand, the active species are not enough to oxidize all BTEX as the concentration of BTEX increased. Furthermore, more intermediate products and by-products are produced with the initial contaminant concentration rising. The generation of intermediate products and by-products inhibits the mineralization and enhances the competitive adsorption [47]. Fu *et al.* [87] found that the removal rate felled slowly when the initial concentration was from 43.6 to 175 mg/m^3. When the concentration of o-xylene was at 218 mg/m^3, the removal rate felled tremendously. The initial toluene concentrations were studied from 300 to 3200 ppm demonstrating that the RE first increased and then decreased with the increase of toluene concentration [97]. More of the adsorbed toluene blocked the formation of hydroxyl radicals on the photocatalyst surface. The effect of the initial concentration of BTEX on photodegradation was demonstrated [122]. As we can see in Fig. 5, when the concentration of BTEX increased from 1 ppm to 5 ppm, the degradation efficiency decreased successively. The reason for this change might be the competition of pollutants and the inhibitory effect of intermediate products or by-products [22].

The flow rate has different effects on the photocatalytic reaction in the continuous mode of operation. The residence time of gas decreases with the increase of airflow rate. Too short residence time will result in low photodegradation efficiency, considering that BTEX gases spend too little time on the catalyst and BTEX does not react adequately [123]. The lower flow rate also reduces convection and diffusion in photocatalytic reactors. On the contrary, too long residence time will lead to the production of a large number of by-products and shorten the service life of the catalyst. Jafari *et al.* [124] discussed the effect of flow rate on toluene decomposition and found that the significantly reduced RE could be attributed to the short contact time. On the other hand, the mass transfer

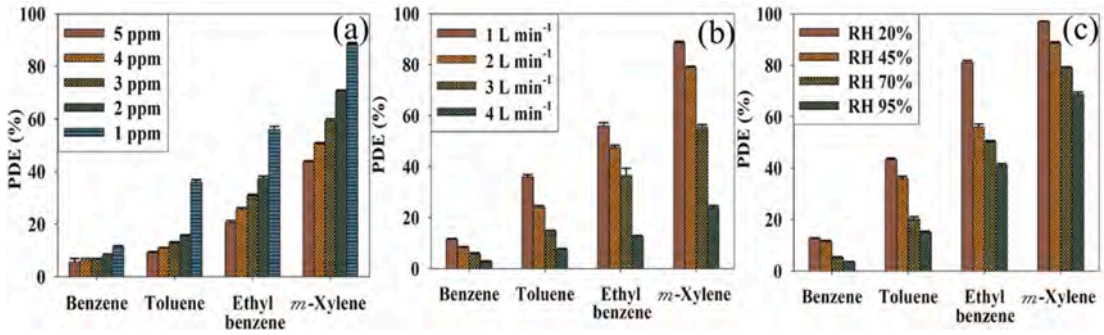

Fig. 5. The photocatalytic degradation efficiencies (PDE) of BTEX using g-C_3N_4/Cu/TNT composite under UV irradiation at different inlet concentrations (a), air flow rates (b), and relative humidity (c) [122].

rate between pollutant and catalyst increases with the gas flow rate increasing. Moreover, the mass transfer promotes the photocatalytic oxidation processes. As the mass transfer rate increase, the removal of pollutants significantly improved [125]. Shayegan *et al.* [126] found that the mass transfer emerges was regarded as the controlling parameter, resulting in the reduction of removal efficiency tinily at the airflow rates between 0.015 and 0.020 m^3/min, respectively. Both the RE and the reaction rates were studied over P25 to investigate the effect of flow rate. When the air flow rate increased from 0.2 to 2 L/min and other operating conditions remain unchanged (concentration of toluene was 3.8 mg/m^3, light intensity was 95 W/m^2, and relative humidity was 25 %), the RE decreased to 10 % of the initial efficiency and the reaction rates were almost constant, which revealed that the surface photocatalytic reactions were the controlling process rather than the gas–solid phase mass transfer [11]. In a word, mass transfer is the main factor in controlling the reaction rate at lower flow rate. However, the effect of residence time was more remarkable in controlling the reaction when the flow rate was higher [47].

3.3. Temperature and relative humidity (RH)

The reaction temperature plays an important role in the photocatalytic process. The higher temperature inhibits the adsorption of pollutants because the adsorption process is usually exothermic, and has a positive impact on the desorption process of intermediate and by-products [78]. In addition, the rise of temperature accelerates the photocatalytic oxidation kinetic reaction according to the Arrhenius formula [79]. Xin *et al.* [47] investigated the toluene photodegradation at different temperatures. And the CuS-CdS/TO_2 showed the best removal efficiency at the reaction temperature of 40℃, which might attribute to the different rate-determining steps at different reaction temperatures. Furthermore, combining thermo-catalysis with photocatalysis to maximize synergistic effects has been widely used for VOCs removal [127,128]. Both the thermal and photo excitation facilitate the effective reaction between reactive oxygen species and BTEX molecules. Yang *et al.* [90] studied that the photothermocatalytic oxidation of toluene was much larger than the single thermo-catalytic or photocatalytic process, suggesting the generation of photo-thermal synergistic catalytic property.

Water molecules are widely present in the atmosphere, especially in all kinds of industrial emissions. In general, the presence of water molecules has a double effect on the photocatalytic oxidation process of BTEX·H_2O as a reactant can generate reactant radical species playing an important part in the oxidation process [41,129]. On the other hand, H_2O may compete with the BTEX and oxygen for adsorption sites on the surface of catalyst [122,130]. At higher humidity, water molecules could connect to OH· present on the photocatalyst surface via hydrogen bond resulting in the formation of multilayer film on the catalyst surface, which can effectively inhibit the photocatalytic degradation of pollutants [79]. Due to the influence of both positive and negative aspects, the degradation efficiency of BTEX showed different trends with the increase of RH. For example, the degradation efficiency increased first and then decreased with the increase of relative humidity in some studies [78,82,126]. However, other researchers found that the degradation efficiency decreased first and then increased as the relative humidity increased [97]. The highest RE of toluene using Ag/TiO_2/CA catalyst was obtained at 45 % humidity, while water may also accelerate the recombination of electron-hole pairs when further increased RH levels, resulting in the inhibition of photocatalytic activity [124]. Zhou *et al.* [131] deduced that high humidity could lead to the annihilation of high-energy electrons and the reduction in the number of electrons owing to the electronegativity of water molecules.

3.4. Light source

The light source has an oversized impact on photocatalytic process of BTEX. First of all, it's worth noting the wavelength of light. Ultraviolet light has a wavelength range of less than 400 nm, while visible light has a wavelength range of 400–760 nm. Generally speaking, there are many photocatalysts, which are insensitive to visible light [43,63,132]. Hence, many researchers have demonstrated the RE of BTEX under UV light was higher than under the visible light [32,133]. The intensity of light also greatly affects the photocatalytic reaction. The enhancement of light intensity in photocatalytic reaction will generate more photon energy and further stimulate the generation of electron hole pairs and the formation of active substances, effectively improving the photocatalytic degradation [97,126]. In addition, BTEX photocatalytic process may produce more byproducts under low light intensity. Fu *et al.* [87] studied the rate of photocatalytic reaction and discovered that the stronger the light intensity, the faster the photocatalytic reaction rate. Oppositely, high light intensity has a negative effect on photocatalytic process, because the recombination rate of electron hole pairs increases with the enlargement of light intensity [124].

3.5. Summary

The photocatalytic degradation of BTEX is collectively affected by different operating conditions. It is difficult to identify-one main role in the photocatalytic degradation of BTEX with the different materials and different reaction mechanisms. Liang's group found that the air flow rate and illumination intensity played the main role on BTEX removal [134]. In the practical application, the air flow rate and the light are more easily adjusted and controlled than other parameters, and it is important to explore the optimal air flow rate and light intensity.

4. Reaction mechanism of BTEX photocatalysis

4.1. Reaction kinetics

The kinetic process of photocatalytic reaction not only determines

the degradation efficiency, but also determines the reaction rate, which is essential to the practical application. It is reported that the process of photo-oxidizing BTEX most widely follows the Langmuir-Hinshelwood (L-H) model [49,135–138]. The BTEX molecules are adsorbed on the surface of catalyst, firstly. And photo-introduced electron-hole pairs may react with O_2 or H_2O adsorbed on the catalyst surface to form surface adsorbed reactive oxygen species. Then the surface adsorbed reactive oxygen species oxidized the adsorbed BTEX molecules. The monomolecular kinetic equation of photocatalytic process forms (Eq. (1)) [138].

$$r = -\frac{dC}{dt} = k\theta = k\frac{KC}{(1+KC)} \tag{1}$$

Where r is the reaction rate, C is the concentration of the reactants in the reaction, θ is the fraction of the reductant adsorbed to the surface, and k and K are the rate constant and the adsorption equilibrium constant, respectively. Qiu's results had a little bit different from the L-H model owing to the shielding effect which ascribed to the higher concentration of pollutants and the generation of intermediate [135]. Furthermore, the monomolecular kinetic equation would be the first-order kinetics when the concentration is very small [139]. When it comes to the competitive adsorption of water, the bimolecular kinetic equation is used in the presence of water vapor [137].

$$r = k\frac{K_1C_1}{1+K_1C_1+K_2C_2} \tag{2}$$

Where K_1 and K_2 are adsorption equilibrium constants of BTEX and water, and C_1 and C_2 are concentrations of BTEX and water in the gas phase, respectively. Yu's group investigated the effect of adsorption on reaction kinetics during photocatalytic degradation of BTEX by the bimolecular kinetic equation [140]. And the relationship between Langmuir adsorption constant (K_1, K_2) and K_H (the Henry's Law constant of VOC) was compared, revealing that there was a positive linear relationship between $1/K_1$ and K_H, and a negative relationship between $1/K_2$ and K_H. Nguyen *et al.* inferred the apparent rate constants during the whole process according to the L-H model, indicating that the efficiency of VOCs increased at low concentrations [139].

4.2. Adsorption

The adsorption on the catalytic surface is an integral part in photocatalytic technology, which is the beginning of the whole reaction. The adsorption of BTEX on TiO_2 was studied using DFT calculations [141]. There were the aromatic π interactions between BTEX and the surfaces, including BTEX- O_{3C} (tri-coordinated oxygen atoms)-TiO_2 and BTEX-Ti_{5C} (Penta-coordinated titanium atoms)-TiO_2. Fig. 6 showed the charge density difference (CDD) between BTEX and TiO_2 anatase. By the calculation, the electron density on the π region of aromatic ring close to the surface of all BTEX increased, revealed that there were the aromatic π interaction in the adsorption of BTEX. The state shifted to a smaller energy for the adsorption on the Ti_{5C} in Fig. 6a and the state remained the same for the adsorption on the O_{3C} indicating that the benzene adsorbent was more stable on Ti_{5C} than O_{3C}, which had the same changes as the adsorption of other BTEX. In addition, there was the hybridization between the d state of Ti_{5C} and carbon p states of benzene. Differently, the methyl hydrogen also played an important influence for xylene on the adsorption process. It was also reported in the literature the adsorption of o-xylene on different surface of TiO_2 suggesting that the stronger adsorption of o-xylene occurred on TiO_2 (0 0 1) rather than TiO_2 (1 0 1) [35].

Chen' group studied the adsorption process on the SnO_2 surface in dark condition using the *in situ* DRIFTs, as shown in Fig. 7 [142]. The benzene and phenol absorption bands were observed in the adsorption process of benzene (Fig. 7a). As shown in Fig. 6b, there were some peaks certified as toluene, benzyl alcohol, benzaldehyde, and benzoic acid in the toluene adsorption process, inferring that those intermediates were produced by chemical adsorption. In o-xylene adsorption process, it was found that o-xylene, o-diphenol and o-phthaladehyde were detected. The chemical adsorption occurred on the SnO_2 surface forming the pre-oxidized products. Furthermore, the adsorption energy on the surface of SnO_2 was calculated by DFT (Fig. 7d-f), indicating that the catalyst showed the best adsorption capacity for o-xylene. The results concluded the presence of methyl groups accelerated the adsorption of BTEX. There were benzyl alcohol, benzaldehyde, and benzoic acid in the adsorption process of toluene on $Sr_2Sb_2O_7$ with abundant surface lattice oxygen

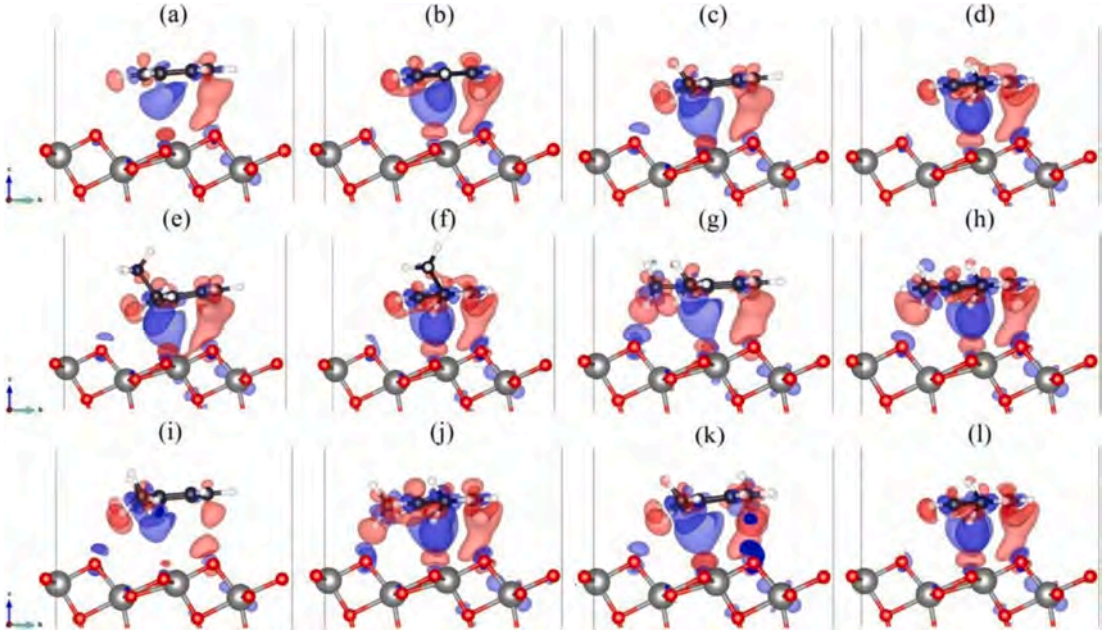

Fig. 6. The CDD of (a) Benzene-Ti_{5C}-anatase; (b) Benzene-O_{3C}-anatase; (c) Toluene-Ti_{5C}-anatase; (d) Toluene-O_{3C}-anatase; (e) Ethylbenzene-Ti_{5C}-anatase; (f) Ethylbenzene-O_{3C}-anatase; (g) o-Xylene-Ti_{5C}-anatase; (h) o-Xylene-O_{3C}-anatase; (i) m-Xylene-Ti_{5C}-anatase; (j) m-Xylene-O_{3C}-anatase; (k) p-Xylene-Ti_{5C}-anatase and (l) p-Xylene-O_{3C}-anatase. Red is for the negative values (electronic density decreased), and blue is for the positive values (electronic density increased). Isosurfaces of 0.0005 e/bohr^3.[29].

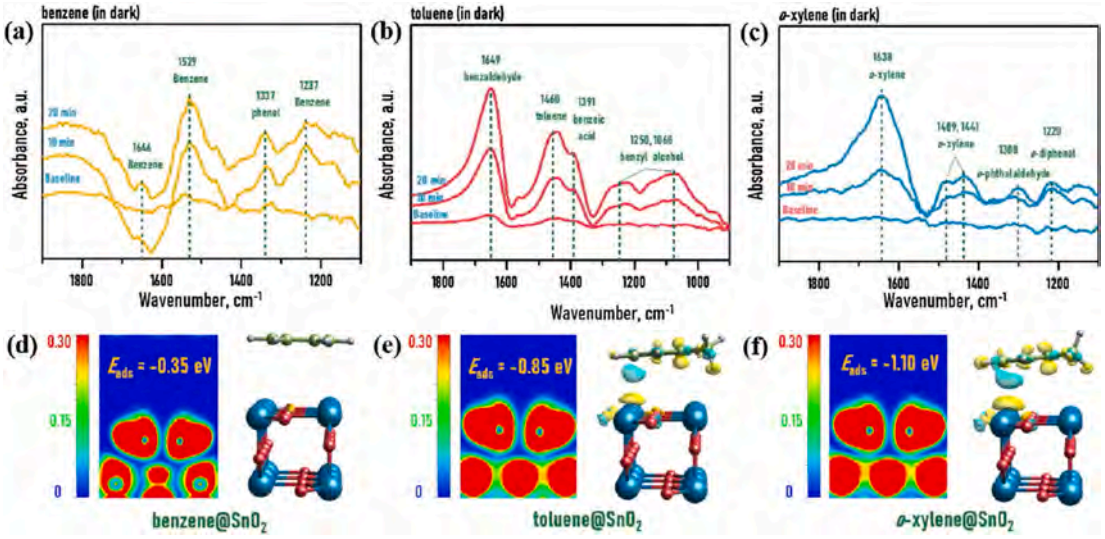

Fig. 7. The adsorption process of benzene, toluene, and o-xylene in dark condition on SnO_2 surface [142].

[143]. Lin *et al.* [144] researched the adsorption behavior of benzene with the presence of H_2O on the TiO_2 catalyst. DFT calculations revealed that the adsorption on the TiO_2 surface was strengthened first and then suppressed as H_2O molecules increased.

4.3. Surface reaction

The photocatalytic reactions are complicated and heterogenetic occurring on the surface of catalysts. Generally speaking, the surface reaction of BTEX is a series of redox reactions, eventually leading to the mineralization of CO_2 and H_2O. In this process, it is inevitable that a lot of intermediates or by-products will be formed [117,145]. It is necessary to study the path and mechanism of photo oxidation reaction of benzene series due to the competitive adsorption of intermediate and by-product [82,106].

4.3.1. Benzene

A series of the radical trapping experiments demonstrated that the

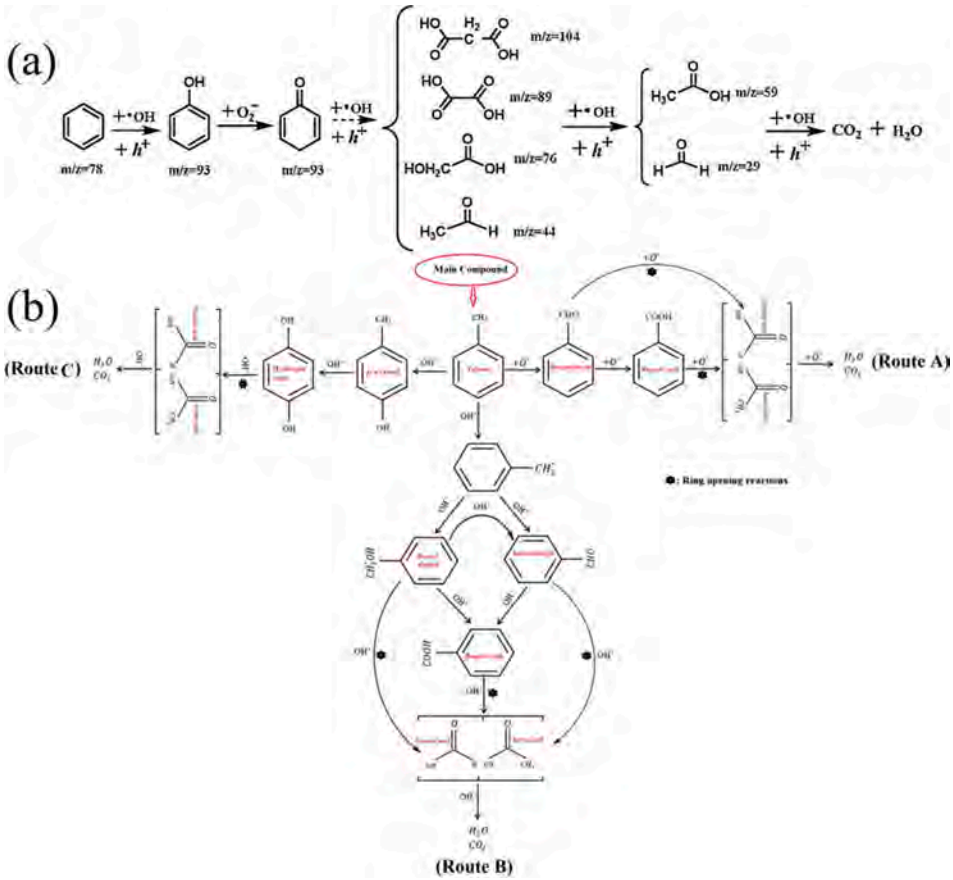

Fig. 8. (a) Photocatalytic degradation pathway of benzene [48]. (b) Photocatalytic degradation pathway of toluene [81].

superoxide radical ($\bullet O_2^-$), hydroxyl radical (•OH) and hole (h^+) were the main radicals in the photodegradation of benzene [146]. As shown in Fig. 8a, the intermediates of benzene were observed during the photocatalytic process using the MS [48]. Firstly, benzene interacted with the •OH and h^+ forming phenol ($m/z = 93$). Benzene was preliminarily attacked by h^+ with the generation of benzene radical cations ($\bullet C_6H_5^+$), and then the $\bullet C_6H_5^+$ reacted with the surface •OH to produce phenol [88]. Other possible paths to form the phenol intermediates from the $\bullet C_6H_5^+$ have also been reported. The $\bullet C_6H_5^+$ was oxide with O_2 or $\bullet O_2^-$ to produce a peroxide reduced to phenol by H^+ [147]. The phenol was oxidized to benzoquinone ($m/z = 93$) by $\bullet O_2^-$ swiftly. Also, there were some peaks identified as p-benzoquinone and o-benzoquinone in some studies, attributing to the further oxidation of phenol [109,148]. Other peaks appeared subsequently identified as malonic acid, oxalic acid, glycolic acid, acetaldehyde, acetic acid, and formaldehyde, which can deduce that the •OH or h^+ opened the benzene ring, forming many organic acids and aldehydes. Finally, all the organic acids and aldehydes were further oxidized to CO_2 and H_2O. Nevertheless, the highly stable coke deposits might be produced by a free radical polymerization on $\bullet C_6H_5^+$. When the surface •OH or H_2O were insufficient, a number of coke deposits would be formed and block the active sites, resulting in the deactivation of catalyst [88].

Moreover, the aromatic ring might open initially in the photocatalytic process. Under the irradiation with a wavelength less than 200 nm, C_6H_6 can dehydrogenate to generated the unsaturated hydrocarbon [149]. And then, the reduction of such unsaturated hydrocarbon was related to the reactive hydrogen. The presence of nonane, decane, and octane revealed that the generated substances interacted with methyl, leading to the emergence of saturated hydrocarbon identified by the GC–MS [148]. The saturated hydrocarbon was oxidized to organic acids and aldehydes and eventually mineralized to CO_2 and H_2O.

4.3.2. Toluene

In previous researches, many intermediates and by-products were identified by the *in situ* FTIR spectra and MS in the photocatalytic process of toluene [100,121]. According to the intermediates and by-products, the possible toluene degradation pathway had been brought up, such as Route A, Route B, Route C (Fig. 8b). In Route A, the toluene was directly oxidized with $\bullet O_2^-$ forming the benzaldehyde and benzoic acid, which were opened the benzene ring to generate low-molecular-weight acids and completely oxidized to CO_2 and H_2O. In Route B, benzyl was the most important intermediate formed by the reaction of toluene and reactive oxygen species (•OH or $\bullet O_2^-$). Then, benzyl possibly was oxidized to benzaldehyde or benzyl alcohol, both of which were eventually oxidized to benzoic acid. Li' group found that the benzoic acid could be ring-opened more easily than the benzaldehyde and benzyl alcohol due to the lowest energy barrier [150]. Furthermore, Dong' group found that the energy barrier for ring-opening of benzoic was lowest, implying that ring opening starting from benzoic acid was observed to be the most favorable for photocatalytic process [151,152]. And the benzyl radicals can react with the toluene forming the dimethyl isophthalate and dimethyl terephthalate [131]. The aromatic compounds were decomposed into CO_2 and H_2O through a series of oxidation, finally. Jafari *et al.* [124] and Liu *et al.* [153] found that the photodegradation path of toluene was consistent with Route B. However, Jafari *et al.* [124] and Cheng *et al.* [121] also found the appearance of CO from the GC–MS instrument, attributing to incomplete oxidation of organic matter. In Route C, p-cresol and hydroquinone emerged by the attack of •OH, and the ring-opening reaction took place sequentially resulting in the formation of low-molecular-weight acids, CO_2 and H_2O. In addition, the photocatalytic process of toluene using the $H_3PW_{12}O_{40}$/g-C_3N_4 film-coated optical fibers might have a different path owing to the emergence of p-hydroxybenzoic acid, 2,4-dihydroxybenzoic acid and succinic acid [117].

4.3.3. Ethylbenzene

As reported in some literatures, Ethylbenzene is generally oxidized more easily than benzene and toluene [29,30,154]. The ethyl group on the benzene ring is more reactive than the methyl group [30]. Hinojosa-Reyes's group found the benzaldehyde and acetophenone in the irradiated gas stream generated by direct photo-oxygenation of organic radicals [155]. Similarly, the ozone-assisted photodegradation pathway for ethylbenzene was investigated by GC–MS and IC [156]. There were nine main types of intermediates in ozone-assisted photodegradation of ethylbenzene, including α-phenylethanol, acetyl benzene, β-phenylethanol, benzyl alcohol, benzaldehyde, benzoic acid, phenol, formic acid and acetic acid. According to the intermediates, the first possible reaction was the oxidation of ethylbenzene by reactive oxygen species forming α-phenylethanol and β-phenylethanol. The further oxidation was occurred with O_3 to produce acetyl benzene and phenylacetic acid, which can remove a formic acid to obtain the benzyl alcohol. And then, the benzyl alcohol was decarboxylated and opened the aromatic ring obtaining some small organic acids. Finally, they were decomposed into CO_2 and H_2O [154].

4.3.4. Xylene

The methyl number in the benzene ring plays an important role in BTEX decomposition. It is unexpected to discover that the activity of BTEX decomposition and quantum efficiency improved with the increase of methyl number [142]. The xylene has three isomerides, including o-xylene, m-xylene and p-xylene. The possible photocatalytic degradation pathways of the three types of xylenes are roughly similar. Under UV–vis light, the possible path ways of photo-oxidizing xylene are diversiform based on the different intermediates analyzed by GC–MS and IR, and there are usually 4 routes. Route 1, the methyl groups of xylene are attacked by •OH or $\bullet O_2^-$ getting 2-benzylalcohol, 2-benzaldehyde, isophthalaldehyde, hydroxybenzoic acid and benzoquinone [35,65,117,154]. And then, those intermediates suffer from ring-opening and decomposition completely. Route 2, the xylene is removed a methyl group to form toluene and even further lose the other methyl to form benzene [65,157]. The removed methyl group might react with hydroxyl to produce formaldehyde [87]. Route 3, the xylene could be isomerized into the other xylene and ethylbenzene by the rearrangement [87,157]. Route 4, the xylene can open the ring directly and split into smaller organic molecules, such as acetylene, allylene, 2-butane, 2-methyl propene, and so on [87,157]. Those organic molecules are mineralized easily to H_2O and CO_2.

5. Practical applications and challenges

5.1. Practical applications

The VOCs discharged from multifarious industries have diverse components and complex nature. And exhaust gas generally has a large gas flow rate. The photocatalytic technology may be under restrictions when the degradation occurs in real conditions, such as higher airflow rate, multi-components. Therefore, it is popular for VOCs removal in practical applications to combine other technologies with photocatalytic technology, which exhibits better efficient removal and lower prices.

5.1.1. Adsorption-photocatalysis combination

The technology of adsorption-photocatalysis combination is the most common in the volatile organic waste gas treatment (Fig. 9a). The adsorption not only reduces the inlet concentration of photocatalysis, but also decreases the emission of products. Moreover, the technology of adsorption-photocatalysis combination degrades the BTEX to CO_2 and H_2O which uses the photocatalysts loading on the adsorption materials. On the one hand, the adsorption materials could enrich the concentration of BTEX before the photocatalysis owing to the larger specific surface area and porous structure. On the other hand, the adsorption may lengthen the residence time resulting in more time for photochemical

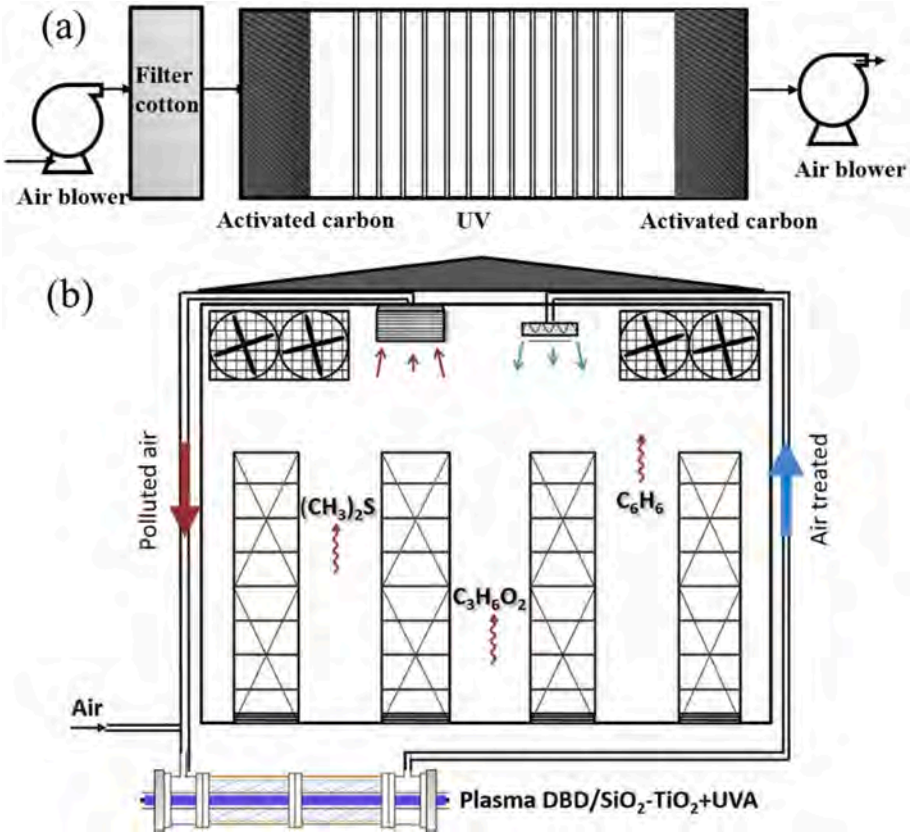

Fig. 9. (a) The typical process flow diagram of VOCs waste gas treatment in the automobile maintenance industry. (b) A hybrid system combining plasma with photocatalysis for treatment [130].

reactions.

The carbon materials are traditional carriers for the rich porous structure and large surface area, comprised of activated carbon (AC), graphene, carbon nanotubes (CNTs), activated carbon fibers (ACFs), and biochar. The TiO_2 films were coated on AC for toluene degradation resulting that the toluene removal efficiency increased 10 % compared the pure TiO_2 [158]. The interaction effect of AC and TiO_2 loading was studied on toluene removal [159]. The degradation efficiency increased initially and then decreased with the TiO_2 and AC loading increasing attributing to the synergetic adsorption-photodegradation effect. ACFs are ideal support materials with microporous structures widely used in photocatalytic processes [160–162]. The addition of ACFs not only improved the performance of degradation greatly, but also prolonged the service life of photocatalysts. Furthermore, molecular sieve is a kind of porous material with strong adsorption capacity and predominant stability. A series of TiO_2 photocatalysts prepared by sol–gel method were germinated in-situ on the surface of ZMS-5 and MCM-41 for benzene degradation [163,164]. The molecular sieve (ZMS-5 and MCM-41) provided high surface area for the dispersion of TiO_2 and accelerated the synergistic adsorption.

5.1.2. *Plasma-photocatalysis combination*

Nowadays, the plasma has attracted extensive attention with superior selectivity and wide range of application. The hard electrons produced by discharging of plasma gas could react with the VOCs in plasma technology. With the assistant of plasma, there are higher concentrations of reactive oxygen species, which could improve the removal efficiency and reduce the emissions of intermediate [165,166]. Benzene was effectively degraded using the non-thermal plasma (NTP) and photocatalytic process in refrigerated food chambers (Fig. 9b) [130]. A synergetic effect between NTP and photocatalysis was observed. In addition, the regeneration of the catalyst by NTP promotes benzene desorption and the degradation of intermediates. The oxygen plasma was applied for removal of VOCs, accelerating the transfer of electrons and forming more reactive oxygen species [56]. Zhu *et al.*[167] studied the degradation of toluene by F-TiO_2/γ-Al_2O_3 coupled with dielectric barrier discharge (DBD) NTP. There were abundant high-energy electrons, ions and free radicals in the DBD-NTP, oxidizing and even mineralizing the byproducts to CO_2 and H_2O.

5.1.3. *Thermo-photocatalysis combination*

The thermo-photocatalysis combination can greatly promote the performance for removing VOCs ascribing the synergistic effect of light energy and heat energy, which is not only conducive to energy saving and improving the stability of the catalyst, but also may improve the selectivity of the target product [127,168]. The photothermal catalytic materials should have a strong whole solar spectral response to achieve the maximum utilization of sunlight. Some researchers have focused mainly on materials responding well to infrared light because the sunlight consists of about 53 % infrared light [169,170]. Combining with the reduced graphene oxide (rGO), the absorption of TiO_2 significantly increased in visible-infrared light, which gave the credit to the electronic interactions between TiO_2 and rGO [169]. Yang' group studied the multifunctional catalyst for thermo-catalytic, photocatalytic and photo-thermo-catalytic oxidation (TCO, PCO and PTO) [90]. The removal efficiency of toluene highly improved in the co-presence of visible-light illumination and heating owing to the lower activation energy and photo-thermal synergy in PTO process. The temperature in toluene removal reduced 40 ℃ under simulated solar irradiation using CeO_2 modified with Fe, attributing to the synergetic effect in PTO process [171]. The photocatalysis can decrease the accumulation of H_2O on catalysts, improving the activity and stability of catalysts.

5.2. Challenges

The stability and sustainable utilization of catalysts are important indexes for practical application. Some photocatalysts reduce their operational lifetime over long periods of exposure and reuse owing to the dirt of the catalysts surface or the instability of the material itself [130,172]. The photocatalysts prepared by Luu' group exhibited instability for decomposition of p-xylene, which activity dropped tremendously [92]. Importantly, the dirt result from the many recalcitrant intermediates which are more powerfully adsorbed on the catalyst than the reactants. The accumulation of the intermediates not only impedes the light absorption but also occupies the active sites resulting in the lack of reactive oxygen species. And the carbon deposits on the surface gives rise to the deactivation of catalysts gradually. Besides, the dehydroxylation on the surface might occur in some photocatalysts leading to reducing their activity because of the consumption of hydroxyl radicals [173]. It is necessary to recover the photocatalytic performance by regeneration techniques after the long-term use of photocatalysts. Generally heating and UV cleaning are admittedly effective methods for the regeneration of catalysts. Xu *et al.* [52] found that heating in 20 vol% H_2/He at 200 ℃ for 0.5 h could effectively regenerate the catalyst. And different regeneration process under the UV irradiation for 1 h in the clean air was adopted by Wu' group, and the photocatalytic activity can return to the original state [174]. Furthermore, combining the photocatalysis and non-thermal plasma (NTP) can put off the fouling on the catalysts' surface, and the adhibition of NTP without the UV irradiation successfully recovered the performance of photocatalysts [130].

6. Conclusions and perspectives

Photocatalytic technology is considered to be the most promising technologies owing to low-energy, and harmlessness. TiO_2, modified with metals, non-metals, or other semiconductors, exhibits superior performance widely noticed and applied to the photocatalytic oxidation of BTEX which not only improves photocatalytic activity, but also prolongs its used life. It is reported that the other metal oxides have a wide band gap and absorption of light, such as ZnO, perovskite oxides, spinel oxides and et al. What's noteworthy is that the hydroxides demonstrated excellent catalytic performance owing to the abundant hydroxyl radicals. In addition, Bi-based photocatalysts, including binary metal oxides, bismuthate and bismuth oxyhalides, and C_3N_4 show the admirable visible light absorption capacity applying to photocatalysis. Furthermore, the operating conditions including the operation mode, initial concentration, airflow rate, temperature, RH and the light were studied adequately. Generally speaking, the photocatalytic process of BTEX mostly follows the L-H model. It is essential to investigate the path of the photocatalytic process for practical application. Although the BTEX have a benzene ring, the degradation pathways differ in details owing to the location and amount of methyl and ethyl groups. In addition, the combination with other technologies and the regeneration of deactivated catalysts are of great significance in practical application.

Although some progresses have been made in the field of photocatalytic degradation about BTEX, there are still many issues that must be solved to meet stringent emission standards in a cost-effective manner. Looking ahead, we consider that the future efforts should be focused on the following aspects.

(1) The heterostructure photocatalysts show superior application prospects, with significantly reduced band gaps and high electron-hole separation. A promising development about photocatalysts with heterojunction should be considered to make full use of the solar spectrum.
(2) Fluid dynamics models and other models can be used to simulate the actual working conditions and design a suitable and efficient reactor according to the influence of operating parameters to overcome the issues in the practical application of photocatalytic degradation of BTEX, such as mass transfer limitations and slow reaction kinetics.
(3) The theoretical calculation (such as DFT) should be combined with experiments to calculate active sites, adsorption energy, and energy barriers of reactions, which can optimize the catalyst structure to improve the performance, determine the reaction rate control steps to improve the reaction rate, and explore the catalyst deactivation problem to promote its effective regeneration.
(4) Most experiments were conducted in the laboratory with higher concentrations and simpler compositions, of which the performance and mechanism were probably different from the realistic working conditions. Therefore, more studies should be carried out in term of photodegradation of mixed VOCs with high flow from industrial processes and highly diluted pollutions from indoor environments.
(5) Developing coupling technologies greatly enhances degradation of BTEX in a more efficient and cost-effective way, including adsorption-photocatalysis, plasma-photocatalysis, and thermo-photocatalysis.

Declaration of Competing Interest

The authors declare that they have no known competing financial interests or personal relationships that could have appeared to influence the work reported in this paper.

Data availability

No data was used for the research described in the article.

Acknowledgements

This work was supported by the Scientific and Technological Major Special Project of Changsha City in China (KQ1201011) , the Key Research and Development Program of Hunan Province in China (2018SK2032, 2018SK2033), and the National Key Research and Development Program of China (2016YFC0204100).

References

[1] C. He, J. Cheng, X. Zhang, M. Douthwaite, S. Pattisson, Z. Hao, Recent advances in the catalytic oxidation of volatile organic compounds: a review based on pollutant sorts and sources, Chem. Rev. 119 (2019) 4471–4568.
[2] S. Maji, G. Beig, R. Yadav, Winter VOCs and OVOCs measured with PTR-MS at an urban site of India: role of emissions, meteorology and photochemical sources, Environ. Pollut. 258 (2020), 113651.
[3] L. Zeng, G. Fan, X. Lyu, H. Guo, J. Wang, D. Yao, Atmospheric fate of peroxyacetyl nitrate in suburban Hong Kong and its impact on local ozone pollution, Environ. Pollut. 252 (2019) 1910–1919.
[4] K.T. Malecha, S.A. Nizkorodov, Photodegradation of secondary organic aerosol particles as a source of small, oxygenated volatile organic compounds, Environ. Sci. Technol. 50 (2016) 9990–9997.
[5] S. Nayek, P.K. Padhy, Personal exposure to VOCs (BTX) and women health risk assessment in rural kitchen from solid biofuel burning during cooking in West Bengal, India, Chemosphere 244 (2020), 125447.
[6] T. An, Y. Huang, G. Li, Z. He, J. Chen, C. Zhang, Pollution profiles and health risk assessment of VOCs emitted during e-waste dismantling processes associated with different dismantling methods, Environ. Int. 73 (2014) 186–194.
[7] Y. Liu, M. Song, X. Liu, Y. Zhang, L. Hui, L. Kong, Y. Zhang, C. Zhang, Y. Qu, J. An, Characterization and sources of volatile organic compounds (VOCs) and their related changes during ozone pollution days in 2016 in Beijing, China, Environ. Pollut. 257 (2020), 113599.
[8] K.W. Fent, C. Toennis, D.L. Sammons, S. Robertson, S.J. Bertke, A.M. Calafat, J. D. Pleil, M.A.G. Wallace, S. Kerber, D.L. Smith, Firefighters' absorption of PAHs and VOCs during controlled residential fires by job assignment and fire attack tactic, J. Exposure Sci. Environ. Epidemiol. (2019) 1–12.
[9] W.S. Choi, M.J. Hwang, Y. Kwon, S. Jung, Y. Youn, M.S. Balathanigaimani, J. Lee, K. Hwang, W. Shim, Radio-frequency thermal plasma treated activated carbon impregnated with Mn and Ag for volatile organic compounds adsorption, J. Nanosci. Nanotechnol. 20 (2020) 4423–4427.

[10] Y. Liu, X. Feng, D. Lawless, Separation of gasoline vapor from nitrogen by hollow fiber composite membranes for VOC emission control, J. Membr. Sci. 271 (2006) 114–124.
[11] L. Zhong, J.J. Brancho, S. Batterman, B.M. Bartlett, C. Godwin, Experimental and modeling study of visible light responsive photocatalytic oxidation (PCO) materials for toluene degradation, Appl. Catal. B 216 (2017) 122–132.
[12] B.D. Napruszewska, A. Michalik-Zym, R. Dula, E. Bielańska, W. Rojek, T. Machej, R.P. Socha, L. Lityńska-Dobrzyńska, K. Bahranowski, E.M. Serwicka, Composites derived from exfoliated Laponite and Mn-Al hydrotalcite prepared in inverse microemulsion: a new strategy for design of robust VOCs combustion catalysts, Appl. Catal. B 211 (2017) 46–56.
[13] E.H. Kim, Y.N. Chun, VOC decomposition by a plasma-cavity combustor, Chem. Eng. Process. Process Intensif. 104 (2016) 51–57.
[14] S.K. Padhi, S. Gokhale, Biological oxidation of gaseous VOCs - rotating biological contactor a promising and eco-friendly technique, J. Environ. Chem. Eng. 2 (2014) 2085–2102.
[15] M.H. Alhaji, K. Sanaullah, S.-F. Lim, A. Khan, C.N. Hipolito, M.O. Abdullah, S. A. Bhawani, T. Jamil, Photocatalytic treatment technology for palm oil mill effluent (POME) - A review, Process Saf. Environ. Prot. 102 (2016) 673–686.
[16] H. Ren, P. Koshy, W. Chen, S. Qi, C.C. Sorrell, Photocatalytic materials and technologies for air purification, J. Hazard. Mater. 325 (2017) 340–366.
[17] Y. Li, W. Ma, Photocatalytic oxidation technology for indoor air pollutants elimination: A review, Chemosphere 280 (2021), 130667.
[18] P.S. Basavarajappa, S.B. Patil, N. Ganganagappa, K.R. Reddy, A.V. Raghu, C. V. Reddy, Recent progress in metal-doped TiO_2, non-metal doped/codoped TiO_2 and TiO_2 nanostructured hybrids for enhanced photocatalysis, Int. J. Hydrogen Energy 45 (2020) 7764–7778.
[19] Y. Li, M. Zhou, B. Cheng, Y. Shao, Recent advances in g-C_3N_4-based heterojunction photocatalysts, J. Mater. Sci. Technol. 56 (2020) 1–17.
[20] A. Talaiekhozani, S. Rezania, K.-H. Kim, R. Sanaye, A.M. Amani, Recent advances in photocatalytic removal of organic and inorganic pollutants in air, J. Cleaner Prod. 278 (2021), 123895.
[21] Z. Shayegan, C.-S. Lee, F. Haghighat, TiO_2 photocatalyst for removal of volatile organic compounds in gas phase - a review, Chem. Eng. J. 334 (2018) 2408–2439.
[22] K. Vikrant, C.M. Park, K.-H. Kim, S. Kumar, E.-C. Jeon, Recent advancements in photocatalyst-based platforms for the destruction of gaseous benzene: performance evaluation of different modes of photocatalytic operations and against adsorption techniques, J. Photochem. Photobiol. C 41 (2019), 100316.
[23] W. Zou, B. Gao, Y.S. Ok, L. Dong, Integrated adsorption and photocatalytic degradation of volatile organic compounds (VOCs) using carbon-based nanocomposites: a critical review, Chemosphere 218 (2019) 845–859.
[24] S. Weon, F. He, W. Choi, Status and challenges in photocatalytic nanotechnology for cleaning air polluted with volatile organic compounds: visible light utilization and catalyst deactivation, Environ. Sci. Nano 6 (2019) 3185–3214.
[25] K. Adam, B. Zuzanna, K. Marta, G. Elżbieta, Z.-G. Agnieszka, J. Marcin, Z. Maciej, Z.-J. Anna, S.-C. Katarzyna, J. Teofil, Microwave -assisted synthesis of a TiO_2-CuO heterojunction with enhanced photocatalytic activity against tetracycline, Appl. Surf. Sci. 520 (2020), 146344.
[26] L. Mo, H. Zheng, Growth of MnO_2 nanoflakes on TiO_2 nanorods for pseudocapacitor, J. Alloy. Compd. 788 (2019) 1162–1168.
[27] K. Fischer, A. Gawel, D. Rosen, M. Krause, A. Abdul Latif, J. Griebel, A. Prager, A. Schulze, Low-temperature synthesis of anatase/rutile/brookite TiO_2 nanoparticles on a polymer membrane for photocatalysis, Catalysts 7 (2017) 209–223.
[28] X. Ma, R. Dang, Z. Liu, F. Yang, H. Li, T. Guo, J. Luo, Facile synthesis of heterogeneous recyclable Pd/CeO_2/TiO_2 nanostructured catalyst for the one pot hydroxylation of benzene to phenol, Chem. Eng. Sci. 211 (2020), 115274.
[29] C.A. Korologos, M.D. Nikolaki, C.N. Zerva, C.J. Philippopoulos, S.G. Poulopoulos, Photocatalytic oxidation of benzene, toluene, ethylbenzene and m-xylene in the gas-phase over TiO_2-based catalysts, J. Photochem. Photobiol. A 244 (2012) 24–31.
[30] L. Laokiat, P. Khemthong, N. Grisdanurak, P. Sreearunothai, W. Pattanasiriwisawa, W. Klysubun, Photocatalytic degradation of benzene, toluene, ethylbenzene, and xylene (BTEX) using transition metal-doped titanium dioxide immobilized on fiberglass cloth, Korean J. Chem. Eng. 29 (2011) 377–383.
[31] S.B. Yang, H.H. Chun, R.J. Tayade, W.K. Jo, Iron-functionalized titanium dioxide on flexible glass fibers for photocatalysis of benzene, toluene, ethylbenzene, and o-xylene (BTEX) under visible- or ultraviolet-light irradiation, J. Air Waste Manag. Assoc. 65 (2015) 365–373.
[32] D. Cherni, N. Moussa, M.F. Nsib, A. Olivo, M. Signoretto, L. Prati, A. Villa, Photocatalytic degradation of ethylbenzene in gas phase over N or NF doped TiO_2 catalysts, J. Mater. Sci. Mater. Electron. 30 (2019) 18919–18926.
[33] Y.Y. Kannangara, R. Wijesena, R.M.G. Rajapakse, K.M.N. de Silva, Heterogeneous photocatalytic degradation of toluene in static environment employing thin films of nitrogen-doped nano-titanium dioxide, International, Nano Lett. 8 (2018) 31–39.
[34] Y. Chen, X. Cao, B. Gao, B. Lin, A facile approach to synthesize N-doped and oxygen-deficient TiO_2 with high visible-light activity for benzene decomposition, Mater. Lett. 94 (2013) 154–157.
[35] A. Mahmood, X. Wang, G. Shi, Z. Wang, X. Xie, J. Sun, Revealing adsorption and the photodegradation mechanism of gas phase o-xylene on carbon quantum dots modified TiO_2 nanoparticles, J. Hazard. Mater. 386 (2020), 121962.
[36] M.-S. Kim, G. Liu, W.K. Nam, B.-W. Kim, Preparation of porous carbon-doped TiO_2 film by sol-gel method and its application for the removal of gaseous toluene in the optical fiber reactor, J. Ind. Eng. Chem. 17 (2011) 223–228.
[37] W.-K. Jo, H.-J. Kang, Aluminum sheet-based S-doped TiO_2 for photocatalytic decomposition of toxic organic vapors, Chin. J. Catal. 35 (2014) 1189–1195.
[38] R. Xie, D. Lei, Y. Zhan, B. Liu, C.H.A. Tsang, Y. Zeng, K. Li, D.Y.C. Leung, H. Huang, Efficient photocatalytic oxidation of gaseous toluene over F-doped TiO_2 in a wet scrubbing process, Chem. Eng. J. 386 (2020), 121025.
[39] Y. Zhang, M. Wu, Y.H. Kwok, Y. Wang, W. Zhao, X. Zhao, H. Huang, D.Y. C. Leung, In-situ synthesis of heterojunction TiO_2/MnO_2 nanostructure with excellent performance in vacuum ultraviolet photocatalytic oxidation of toluene, Appl. Catal. B 259 (2019), 118034.
[40] X. Dai, G. Lu, Y. Hu, X. Xie, X. Wang, J. Sun, Reversible redox behavior of Fe_2O_3/TiO_2 composites in the gaseous photodegradation process, Ceram. Int. 45 (2019) 13187–13192.
[41] W. Zhou, B. Shen, F. Wang, X. Zhang, Z. Zhao, M. Si, S. Guo, Enhanced photocatalytic degradation of xylene by blackening TiO_2 nanoparticles with high dispersion of CuO, J. Hazard. Mater. 391 (2020), 121642.
[42] L. Zhang, M. Qin, W. Yu, Q. Zhang, H. Xie, Z. Sun, Q. Shao, X. Guo, L. Hao, Y. Zheng, Z. Guo, Heterostructured TiO_2/WO_3 nanocomposites for photocatalytic degradation of toluene under visible light, J. Electrochem. Soc. 164 (2017) H1086–H1090.
[43] X. Wang, M. Sun, M. Murugananthan, Y. Zhang, L. Zhang, Electrochemically self-doped WO_3/TiO_2 nanotubes for photocatalytic degradation of volatile organic compounds, Appl. Catal. B 260 (2020), 118205.
[44] J. Kong, X. Lai, Z. Rui, H. Ji, S. Ji, Multichannel charge separation promoted ZnO/P25 heterojunctions for the photocatalytic oxidation of toluene, Chin. J. Catal. 37 (2016) 869–877.
[45] V.B. Koli, J.-S. Kim, Photocatalytic oxidation for removal of gases toluene by TiO_2-CeO_2 nanocomposites under UV light irradiation, Mater. Sci. Semicond. Process. 94 (2019) 70–79.
[46] J. Qu, D. Chen, N. Li, Q. Xu, H. Li, J. He, J. Lu, Ternary photocatalyst of atomic-scale Pt coupled with MoS_2 co-loaded on TiO_2 surface for highly efficient degradation of gaseous toluene, Appl. Catal. B 256 (2019), 117877.
[47] Y. Xin, Q. Chen, G. Zhang, Construction of ternary heterojunction CuS-CdS/TiO_2 nanobelts for photocatalytic degradation of gaseous toluene, J. Alloy. Compd. 751 (2018) 231–240.
[48] J. Hua, M. Wang, Y. Jiao, H. Li, Y. Yang, Strongly coupled CdX (X S, Se and Te) quantum dots/TiO_2 nanocomposites for photocatalytic degradation of benzene under visible light irradiation, Optik 171 (2018) 95–106.
[49] U. Caudillo-Flores, M.J. Muñoz-Batista, R. Luque, M. Fernández-García, A. Kubacka, g-C_3N_4/TiO_2 composite catalysts for the photo-oxidation of toluene: chemical and charge handling effects, Chem. Eng. J. 378 (2019), 122228.
[50] H. Huang, D. Li, Q. Lin, W. Zhang, Y. Shao, Y. Chen, M. Sun, X. Fu, Efficient degradation of benzene over $LaVO_4$/TiO_2 nanocrystalline heterojunction photocatalyst under visible light irradiation, Environ. Sci. Technol. 43 (2009) 4164–4168.
[51] H. Huang, H. Huang, L. Zhang, P. Hu, X. Ye, D.Y.C. Leung, Enhanced degradation of gaseous benzene under vacuum ultraviolet (VUV) irradiation over TiO_2 modified by transition metals, Chem. Eng. J. 259 (2015) 534–541.
[52] T. Xu, H. Zheng, P. Zhang, Isolated Pt single atomic sites anchored on nanoporous TiO_2 film for highly efficient photocatalytic degradation of low concentration toluene, J. Hazard. Mater. 388 (2020), 121746.
[53] J.Y. Lee, J.H. Choi, Sonochemical synthesis of Ce-doped TiO_2 nanostructure: a visible-light-driven photocatalyst for degradation of toluene and o-xylene, Materials (Basel) 12 (2019) 1–14.
[54] S. Sun, J. Ding, J. Bao, C. Gao, Z. Qi, X. Yang, B. He, C. Li, Photocatalytic degradation of gaseous toluene on Fe-TiO_2 under visible light irradiation: a study on the structure, activity and deactivation mechanism, Appl. Surf. Sci. 258 (2012) 5031–5037.
[55] T.D. Pham, B.K. Lee, Novel adsorption and photocatalytic oxidation for removal of gaseous toluene by V-doped TiO_2/PU under visible light, J. Hazard. Mater. 300 (2015) 493–503.
[56] X.-S. Li, X.-Y. Ma, J.-L. Liu, Z.-G. Sun, B. Zhu, A.-M. Zhu, Plasma-promoted Au/TiO_2 nanocatalysts for photocatalytic formaldehyde oxidation under visible-light irradiation, Catal. Today 337 (2019) 132–138.
[57] X. Zhu, C. Jin, X.-S. Li, J.-L. Liu, Z.-G. Sun, C. Shi, X. Li, A.-M. Zhu, Photocatalytic formaldehyde oxidation over plasmonic Au/TiO_2 under visible light: moisture indispensability and light enhancement, ACS Catal. 7 (2017) 6514–6524.
[58] M. Xu, Y. Wang, J. Geng, D. Jing, Photodecomposition of NOx on Ag/TiO_2 composite catalysts in a gas phase reactor, Chem. Eng. J. 307 (2017) 181–188.
[59] M. Stucchi, C.L. Bianchi, C. Pirola, G. Cerrato, S. Morandi, C. Argirusis, G. Sourkouni, A. Naldoni, V. Capucci, Copper NPs decorated titania: a novel synthesis by high energy US with a study of the photocatalytic activity under visible light, Ultrason. Sonochem. 31 (2016) 295–301.
[60] S. Saqlain, B.J. Cha, S.Y. Kim, T.K. Ahn, C. Park, J.-M. Oh, E.C. Jeong, H.O. Seo, Y. D. Kim, Visible light-responsive Fe-loaded TiO_2 photocatalysts for total oxidation of acetaldehyde: Fundamental studies towards large-scale production and applications, Appl. Surf. Sci. 505 (2020), 144160.
[61] M. Chen, H. Wang, X. Chen, F. Wang, X. Qin, C. Zhang, H. He, High-performance of Cu-TiO_2 for photocatalytic oxidation of formaldehyde under visible light and the mechanism study, Chem. Eng. J. 390 (2020), 124481.
[62] Z. Rao, X. Xie, X. Wang, A. Mahmood, S. Tong, M. Ge, J. Sun, Defect chemistry of Er^{3+}-doped TiO_2 and its photocatalytic activity for the degradation of flowing gas-phase VOCs, J. Phys. Chem. C 123 (2019) 12321–12334.
[63] L. Tian, L. Xing, X. Shen, Q. Li, S. Ge, B. Liu, L. Jie, Visible light enhanced Fe-I-TiO_2 photocatalysts for the degradation of gaseous benzene, Atmos. Pollut. Res. 11 (2020) 179–185.

[64] I. Wysocka, A. Markowska-Szczupak, P. Szweda, J. Ryl, M. Endo-Kimura, E. Kowalska, G. Nowaczyk, A. Zielinska-Jurek, Gas-phase removal of indoor volatile organic compounds and airborne microorganisms over mono- and bimetal-modified (Pt, Cu, Ag) titanium(IV) oxide nanocomposites, Indoor Air 29 (2019) 979–992.

[65] Z. Rao, G. Shi, Z. Wang, A. Mahmood, X. Xie, J. Sun, Photocatalytic degradation of gaseous VOCs over Tm^{3+}-TiO_2: revealing the activity enhancement mechanism and different reaction paths, Chem. Eng. J. 395 (2020), 125078.

[66] X. Lei, X. Xue, H. Yang, C. Chen, X. Li, M. Niu, X. Gao, Y. Yang, Effect of calcination temperature on the structure and visible-light photocatalytic activities of (N, S and C) co-doped TiO_2 nano-materials, Appl. Surf. Sci. 332 (2015) 172–180.

[67] B. Tryba, M. Wozniak, G. Zolnierkiewicz, N. Guskos, A. Morawski, C. Colbeau-Justin, R. Wrobel, A. Nitta, B. Ohtani, Influence of an electronic structure of N-TiO_2 on its photocatalytic activity towards decomposition of acetaldehyde under UV and fluorescent lamps irradiation, Catalysts 8 (2018) 85.

[68] R. Kavitha, L.G. Devi, Synergistic effect between carbon dopant in titania lattice and surface carbonaceous species for enhancing the visible light photocatalysis, J. Environ. Chem. Eng. 2 (2014) 857–867.

[69] M. Li, W. Song, L. Zeng, D. Zeng, C. Xie, Q. Yang, Mechanistic study of N-H- and H-N-codoping of a TiO_2 photocatalyst for efficient degradation of benzene under visible light, RSC Adv. 10 (2020) 2757–2766.

[70] C. Di Valentin, G. Pacchioni, Trends in non-metal doping of anatase TiO_2: B, C, N and F, Catal. Today 206 (2013) 12–18.

[71] B. Li, X. Cheng, X. Yu, L. Yan, Z. Xing, Synthesis and characterization of Fe-N-S-tri-doped TiO_2 photocatalyst and its enhanced visible light photocatalytic activity, Adv. Mater. Sci. Eng. 2012 (2012) 1–5.

[72] X. He, J. Zhu, L. Tan, H. Wang, M. Zhou, Visible light-induced photocatalytic degradation of gaseous toluene by Ce, S and N doped ionic liquid-TiO_2, Mater. Sci. Semicond. Process. 120 (2020), 105259.

[73] C.W. Dunnill, I.P. Parkin, Nitrogen-doped TiO_2 thin films: photocatalytic applications for healthcare environments, Dalton Trans. 40 (2011) 1635–1640.

[74] N. Talinungsang, D.D. Paul, M.G. Purkayastha, Krishna, TiO_2/SnO_2 and SnO_2/TiO_2 heterostructures as photocatalysts for degradation of stearic acid and methylene blue under UV irradiation, Superlattices Microstruct. 129 (2019) 105–114.

[75] Y. Wang, Q. Wang, X. Zhan, F. Wang, M. Safdar, J. He, Visible light driven type II heterostructures and their enhanced photocatalysis properties: a review, Nanoscale 5 (2013) 8326–9339.

[76] W. Gao, X. Zhang, X. Su, F. Wang, Z. Liu, B. Liu, J. Zhan, H. Liu, Y. Sang, Construction of bimetallic Pd-Ag enhanced AgBr/TiO_2 hierarchical nanostructured photocatalytic hybrid capillary tubes and devices for continuous photocatalytic degradation of VOCs, Chem. Eng. J. 346 (2018) 77–84.

[77] P. Wu, S. Dai, G. Chen, S. Zhao, Z. Xu, M. Fu, P. Chen, Q. Chen, X. Jin, Y. Qiu, S. Yang, D. Ye, Interfacial effects in hierarchically porous α-MnO_2/Mn_3O_4 heterostructures promote photocatalytic oxidation activity, Appl. Catal. B 268 (2020), 118418.

[78] A.J. Jafari, R.R. Kalantari, M. Kermani, M.H. Firooz, Photocatalytic oxidation of benzene by ZnO coated on glass plates under simulated sunlight, Chem. Pap. 73 (2019) 635–644.

[79] A.J. Jafari, R.R. Kalantari, M. Kermani, M.H. Firooz, ZnO nanoparticles photocatalytic activity toward atmospheric toluene under simulated sunlight, Res. Chem. Intermed. 46 (2019) 119–131.

[80] J. Liu, P. Wang, W. Qu, H. Li, L. Shi, D. Zhang, Nanodiamond-decorated ZnO catalysts with enhanced photocorrosion-resistance for photocatalytic degradation of gaseous toluene, Appl. Catal. B 257 (2019), 117880.

[81] A.J. Jafari, H. Arfaeinia, B. Ramavandi, R.R. Kalantary, A. Esrafily, Ozone-assisted photocatalytic degradation of gaseous toluene from waste air stream using silica-functionalized graphene oxide/ZnO coated on fiberglass: performance, intermediates, and mechanistic pathways, Air Qual. Atmos. Health 12 (2019) 1181–1188.

[82] A.J. Jafari, R.R. Kalantary, A. Esrafili, H. Arfaeinia, Synthesis of silica-functionalized graphene oxide/ZnO coated on fiberglass and its application in photocatalytic removal of gaseous benzene, Process Saf. Environ. Prot. 116 (2018) 377–387.

[83] A. Changsuphan, M.I.B.A. Wahab, N.T. Kim Oanh, Removal of benzene by ZnO nanoparticles coated on porous adsorbents in presence of ozone and UV, Chem. Eng. J. (2012).

[84] J. Zhou, M. Wu, Y. Zhang, C. Zhu, Y. Fang, Y. Li, L. Yu, 3D hierarchical structures MnO_2/C: a highly efficient catalyst for purification of volatile organic compounds with visible light irradiation, Appl. Surf. Sci. 447 (2018) 191–199.

[85] M. Wu, Y. Zhang, W. Szeto, W. Pan, H. Huang, D.Y.C. Leung, Vacuum ultraviolet (VUV)-based photocatalytic oxidation for toluene degradation over pure CeO_2, Chem. Eng. Sci. 200 (2019) 203–213.

[86] S. Wang, Y. Guan, R. Zeng, Z. Zhang, L. Liu, Z. Li, W. An, Y. Fu, Plate-like WO_3 inserting into I-deficient $BiO_{1.2}I_{0.6}$ microsphere for highly efficient photocatalytic degradation of VOCs, J. Taiwan Inst. Chem. Eng. 105 (2019) 96–103.

[87] S. Fu, Y. Zheng, X. Zhou, Z. Ni, S. Xia, Visible light promoted degradation of gaseous volatile organic compounds catalyzed by Au supported layered double hydroxides: influencing factors, kinetics and mechanism, J. Hazard. Mater. 363 (2019) 41–54.

[88] D. Huang, X. Fu, J. Long, X. Jiang, L. Chang, S. Meng, S. Chen, Hydrothermal synthesis of $MSn(OH)_6$ (M=Co, Cu, Fe, Mg, Mn, Zn) and their photocatalytic activity for the destruction of gaseous benzene, Chem. Eng. J. 269 (2015) 168–179.

[89] B.-G. Park, Photoluminescence of Eu^{3+}-doped $CaTiO_3$ perovskites and their photocatalytic properties with a metal ion loading, Chem. Phys. Lett. 722 (2019) 44–49.

[90] X. Yang, S. Liu, J. Li, J. Chen, Z. Rui, Promotion effect of strong metal-support interaction to thermocatalytic, photocatalytic, and photothermocatalytic oxidation of toluene on Pt/$SrTiO_3$, Chemosphere 249 (2020), 126096.

[91] M. Miodyńska, B. Bajorowicz, P. Mazierski, W. Lisowski, T. Klimczuk, M. J. Winiarski, A. Zaleska-Medynska, J. Nadolna, Preparation and photocatalytic properties of $BaZrO_3$ and $SrZrO_3$ modified with Cu_2O/Bi_2O_3 quantum dots, Solid State Sci. 74 (2017) 13–23.

[92] C.L. Luu, T.T. Van Nguyen, T. Nguyen, P.A. Nguyen, T.C. Hoang, C.A. Ha, Thin film nano-photocatalyts with low band gap energy for gas phase degradation of p-xylene: TiO_2 doped Cr, UiO66-NH2 and LaBO3 (B = Fe, Mn, and Co), Adv. Nat. Sci. Nanosci. Nanotechnol. 9 (2017) 1–8.

[93] S.S. Jamali, D. Singh, H. Tavakkoli, F. Kaveh, T. Tabari, Microwave-assisted synthesis of nanostructured perovskite-type oxide with efficient photocatalytic activity against organic reactants in gaseous and aqueous phases, Mater. Sci. Semicond. Process. 64 (2017) 47–54.

[94] B. Bajorowicz, J. Nadolna, W. Lisowski, T. Klimczuk, A. Zaleska-Medynska, The effects of bifunctional linker and reflux time on the surface properties and photocatalytic activity of CdTe quantum dots decorated $KTaO_3$ composite photocatalysts, Appl. Catal. B 203 (2017) 452–464.

[95] A. Krukowska, G. Trykowski, W. Lisowski, T. Klimczuk, M.J. Winiarski, A. Zaleska-Medynska, Monometallic nanoparticles decorated and rare earth ions doped $KTaO_3$/$K_2Ta_2O_6$ photocatalysts with enhanced pollutant decomposition and improved H_2 generation, J. Catal. 364 (2018) 371–381.

[96] A. Krukowska, G. Trykowski, M.J. Winiarski, T. Klimczuk, W. Lisowski, A. Mikolajczyk, H.P. Pinto, A. Zaleska-Medynska, Mono- and bimetallic nanoparticles decorated $KTaO_3$ photocatalysts with improved Vis and UV-Vis light activity, Appl. Surf. Sci. 441 (2018) 993–1011.

[97] H. Mehrizadeh, A. Niaei, H.-H. Tseng, D. Salari, A. Khataee, Synthesis of $ZnFe_2O_4$ nanoparticles for photocatalytic removal of toluene from gas phase in the annular reactor, J. Photochem. Photobiol. A 332 (2017) 188–195.

[98] Z. Yin, B. Liu, S. Fan, P. Wang, X. Wang, D. Long, L. Zhang, X. Yang, X. Li, In situ FTIR spectra investigation of the photocatalytic degradation of gaseous toluene over a novel hedgehog-like $CaFe_2O_4$ hollow-structured materials, Catal. Commun. 130 (2019), 105754.

[99] M. Sun, D. Li, W. Zhang, Z. Chen, H. Huang, W. Li, Y. He, X. Fu, Rapid microwave hydrothermal synthesis of $ZnGa_2O_4$ with high photocatalytic activity toward aromatic compounds in air and dyes in liquid water, J. Solid State Chem. 190 (2012) 135–142.

[100] Q. Zhou, Q. Zhao, W. Xiong, X. Li, J. Li, L. Zeng, Hollow porous zinc cobaltate nanocubes photocatalyst derived from bimetallic zeolitic imidazolate frameworks towards enhanced gaseous toluene degradation, J. Colloid Interface Sci. 516 (2018) 76–85.

[101] S. Zhang, W. Pu, A. Chen, Y. Xu, Y. Wang, C. Yang, J. Gong, Oxygen vacancies enhanced photocatalytic activity towards VOCs oxidation over Pt deposited Bi_2WO_6 under visible light, J. Hazard. Mater. 384 (2020), 121478.

[102] Y. Liu, C. Zhu, J. Sun, Y. Ge, F. Song, Q. Xu, In situ assembly of CQDs/Bi_2WO_6 for highly efficient photocatalytic degradation of VOCs under visible light, New J. Chem. 44 (2020) 3455–3462.

[103] J. Cheng, S. Shi, T. Tang, S. Tian, W. Yang, D. Zeng, Controllable topological transformation from BiOCl hierarchical microspheres to Bi_2WO_6 superstructures in the Bi-W-Cl-O system, J. Alloy. Compd. 643 (2015) 159–166.

[104] X.a. Dong, W. Cui, H. Wang, J. Li, Y. Sun, H. Wang, Y. Zhang, H. Huang, F. Dong, Promoting ring-opening efficiency for suppressing toxic intermediates during photocatalytic toluene degradation via surface oxygen vacancies, Sci. Bull. 64 (2019) 669-678.

[105] R. Sun, Q. Shi, M. Zhang, L. Xie, J. Chen, X. Yang, M. Chen, W. Zhao, Enhanced photocatalytic oxidation of toluene with a coral-like direct Z-scheme $BiVO_4$ /g-C_3N_4 photocatalyst, J. Alloy. Compd. 714 (2017) 619–626.

[106] J. Duan, X. Song, H. Zhao, Z. Zhang, W. Wang, Self-assembled flower-like $(BiO)_2CO_3$-CdS-CuS stable heterojunction degrades toluene under visible light response, Opt. Mater. 101 (2020), 109761.

[107] C.B. Ong, L.Y. Ng, A.W. Mohammad, A review of ZnO nanoparticles as solar photocatalysts: synthesis, mechanisms and applications, Renew. Sustain. Energy Rev. 81 (2018) 536–551.

[108] X. Zou, S. Zhao, J. Zhang, H. Sun, Q. Pan, Y. Guo, Preparation of ternary ZnO/Ag/cellulose and its enhanced photocatalytic degradation property on phenol and benzene in VOCs, Open Chem. 17 (2019) 779–787.

[109] T. Odoom-Wubah, Q. Li, Q. Wang, M.Z. Rukhsana Usha, J. Huang, Q. Li, Template-free synthesis of carbon self-doped ZnO superstructures as efficient support for ultra fine Pd nanoparticles and their catalytic activity towards benzene oxidation, Mol. Catal. 469 (2019) 118–130.

[110] X. Zhang, J. Qin, Y. Xue, P. Yu, B. Zhang, L. Wang, R. Liu, Effect of aspect ratio and surface defects on the photocatalytic activity of ZnO nanorods, Sci. Rep. 4 (2014) 1–8.

[111] T. Montini, M. Melchionna, M. Monai, P. Fornasiero, Fundamentals and catalytic applications of CeO_2-based materials, Chem. Rev. 116 (2016) 5987–6041.

[112] J. Gao, Z. Si, Y. Xu, L. Liu, Y. Zhang, X. Wu, R. Ran, D. Weng, Pd-Ag@CeO_2 catalyst of core-shell structure for low temperature oxidation of toluene under visible light irradiation, J. Phys. Chem. C 123 (2018) 1761–1769.

[113] S. Higashimoto, K. Katsuura, M. Yamamoto, M. Takahashi, Photocatalytic activity for decomposition of volatile organic compound on Pt-WO_3 enhanced by simple physical mixing with TiO_2, Catal. Commun. 133 (2020), 105831.

[114] H. Wang, B. Liao, T. Lu, Y. Ai, G. Liu, Enhanced visible-light photocatalytic degradation of tetracycline by a novel hollow BiOCl@CeO_2 heterostructured microspheres: structural characterization and reaction mechanism, J. Hazard. Mater. 385 (2020), 121552.

[115] R. Parvari, F. Ghorbani-Shahna, A. Bahrami, S. Azizian, M.J. Assari, M. Farhadian, A novel core-shell structured α-Fe_2O_3/Cu/g-C_3N_4 nanocomposite for continuous photocatalytic removal of air ethylbenzene under visible light irradiation, J. Photochem. Photobiol. A 399 (2020), 112643.

[116] C. Zhao, H. Jia, W. Jin, F. Li, H. Li, W. Chen, TiO_2 nanoparticles and CQDs co-decorated mesoporous g-C_3N_4 and their photocatalytic properties for gaseous benzene degradation, Funct. Mater. Lett. 12 (2019) 1950086.

[117] J. Meng, X. Wang, X. Yang, A. Hu, Y. Guo, Y. Yang, Enhanced gas-phase photocatalytic removal of aromatics over direct Z-scheme-dictated $H_3PW_{12}O_{40}$/g-C_3N_4 film-coated optical fibers, Appl. Catal. B 251 (2019) 168–180.

[118] F. Khodadadian M.W.d. Boer, A. Poursaeidesfahani, J.R.v. Ommen, A.I. Stankiewicz, R. Lakerveld, Design, characterization and model validation of a LED-based photocatalytic reactor for gas phase applications Chemical Engineering Journal 333 2018 456 466.

[119] N.L.M. Tri, D.S. Duc, D. Van Thuan, T.A. Tahtamouni, T.-D. Pham, D.T. Tran, N. Thi Phuong Le Chi, V.N. Nguyen, Superior photocatalytic activity of Cu doped $NiWO_4$ for efficient degradation of benzene in air even under visible radiation, Chem. Phys. 525 (2019) 110411.

[120] J.E. Cuthrell, L.T. Biegler, Simultaneous optimization and solution methods for batch reactor control profiles, Comput. Chem. Eng. 13 (1989) 49–62.

[121] Z. Cheng, C. Li, D. Chen, J. Chen, S. Zhang, J. Ye, J. Yu, D.D. Dionysiou, A novel array of double dielectric barrier discharge combined with TiCo catalyst to remove high-flow-rate toluene: performance evaluation and mechanism analysis, Sci. Total Environ. 692 (2019) 940–951.

[122] D.J. Kim, W.-K. Jo, Mitigation of harmful indoor organic vapors using plug-flow unit coated with 2D g-C_3N_4 and metallic Cu dual-incorporated 1D titania heterostructure, Chemosphere 202 (2018) 184–190.

[123] N.L. Minh Tri, K. Jitae, D. Van Thuan, P. Thi Huong, T.M. Al Tahtamouni, Improved photocatalytic decomposition of methyl ethyl ketone gas from indoor air environment by using TiO_2/graphene oxide, Mater. Res. Express 6 (2019) 1–30.

[124] A. Jonoidi Jafari, M. Kermani, A. Hosseini-Bandegharaei, A. Rastegar, M. Gholami, A. Alahabadi, G. Farzi, Synthesis and characterization of Ag/TiO_2/ composite aerogel for enhanced adsorption and photo-catalytic degradation of toluene from the gas phase, Chem. Eng. Res. Des. 150 (2019) 1–13.

[125] I. Dundar, M. Krichevskaya, A. Katerski, M. Krunks, I. Oja Acik, Photocatalytic degradation of different VOCs in the gas-phase over TiO_2 thin films prepared by ultrasonic spray pyrolysis, Catalysts 9 (2019) 915–933.

[126] Z. Shayegan, C.-S. Lee, F. Haghighat, Effect of surface fluorination of P25-TiO_2 coated on nickel substrate for photocatalytic oxidation of methyl ethyl ketone in indoor environments, J. Environ. Chem. Eng. 7 (2019), 103390.

[127] J. Kong, Z. Xiang, G. Li, T. An, Introduce oxygen vacancies into CeO_2 catalyst for enhanced coke resistance during photothermocatalytic oxidation of typical VOCs, Appl. Catal. B 269 (2020), 118755.

[128] X. Xie, Y. Li, Y. Yang, C. Chen, Q. Zhang, UV-Vis-IR driven thermocatalytic activity of OMS-2/SnO_2 nanocomposite significantly enhanced by novel photoactivation and synergetic photocatalysis-thermocatalysis, Appl. Surf. Sci. 462 (2018) 590–597.

[129] H. Ye, Z. Wang, Y. Liu, S. Chen, H. Wang, Z. Wu, Efficient degradation of gas-phase toluene by ozone-assisted photocatalytic oxidation on TiO_2/graphene composites, Catal. Lett. 149 (2019) 2739–2748.

[130] T. Zadi, M. Azizi, N. Nasrallah, A. Bouzaza, R. Maachi, D. Wolbert, S. Rtimi, A. A. Assadi, Indoor air treatment of refrigerated food chambers with synergetic association between cold plasma and photocatalysis: process performance and photocatalytic poisoning, Chem. Eng. J. 382 (2020), 122951.

[131] W. Zhou, Z. Guan, M. Zhao, J. Li, Characteristics and mechanism of toluene removal from gas by novelty array double dielectric barrier discharge combined with TiO_2/Al_2O_3 catalyst, Chemosphere 226 (2019) 766–773.

[132] G. Huang, S. Li, L. Liu, L. Zhu, Q. Wang, Ti_3C_2 MXene-modified Bi_2WO_6 nanoplates for efficient photodegradation of volatile organic compounds, Appl. Surf. Sci. 503 (2020), 144183.

[133] F. Azimi, R. Nabizadeh, M.S. Hassanvand, N. Rastkari, S. Nazmara, K. Naddafi, Photochemical degradation of toluene in gas-phase under UV/visible light graphene oxide-TiO_2 nanocomposite: influential operating factors, optimization, and modeling, J. Environ. Health Sci. Eng. 17 (2019) 671–683.

[134] C. Liang, C. Li, Y. Zhu, X. Du, Y. Zeng, Y. Zhou, J. Zhao, S. Li, X. Liu, Q. Yu, Y. Zhai, Light-driven photothermal catalysis for degradation of toluene on CuO/TiO_2 Composite: Dominating photocatalysis and auxiliary thermalcatalysis, Appl. Surf. Sci. 601 (2022).

[135] L. Qiu, H. Li, F. Dai, F. Ouyang, D. Pang, H. Wang, Adsorption and photocatalytic degradation of benzene compounds on acidic F-TiO_2/SiO_2 catalyst, Chemosphere 246 (2020), 125698.

[136] A. Khalilzadeh, S. Fatemi, Spouted bed reactor for VOC removal by modified nano-TiO_2 photocatalytic particles, Chem. Eng. Res. Des. 115 (2016) 241–250.

[137] V. Nguyen Thi Thuy, L. Luu Cam, T. Nguyen, A. Nguyen Phung, A. Ha Cam, T. Nguyen Thanh, D. Nguyen Lam Thuy, C. Hoang Tien, Kinetics of photocatalytic degradation of gaseous p-xylene on UiO-66-NH2 and $LaFeO_3$ thin films under combined illumination of ultraviolet and visible lights, Int. J. Chem. Kinet. 52 (2019) 35-51.

[138] C.L. Luu, Q.T. Nguyen, T. Nguyen, S.T. Ho, Kinetics of gas-phase photooxidation of p-xylene on nano TiO_2 P25 thin film, Adv. Nat. Sci. Nanosci. Nanotechnol. 9 (2018) 1–12.

[139] A.T. Nguyen, R.-S. Juang, Photocatalytic degradation of p-chlorophenol by hybrid H_2O_2 and TiO_2 in aqueous suspensions under UV irradiation, J. Environ. Manage. 147 (2015) 271–277.

[140] K.-P. Yu, G.W.M. Lee, W.-M. Huang, C. Wu, S. Yang, The correlation between photocatalytic oxidation performance and chemical/physical properties of indoor volatile organic compounds, Atmos. Environ. 40 (2006) 375–385.

[141] M. Dos Reis Vargas, E.A.S. De Castro, J. Politi, R. Gargano, J.B.L. Martins, BTEX adsorption on TiO_2 anatase and rutile surfaces: DFT functionals, J. Mol. Model. 25 (2019) 137.

[142] R. Chen, J. Li, J. Sheng, W. Cui, X.a., Dong,, P., Chen,, H., Wang,, Y., Sun,, F., Dong,, Unveiling the unconventional roles of methyl number on the ring-opening barrier in photocatalytic decomposition of benzene, toluene and o-xylene, Appl. Catal. B 278 (2020), 119318.

[143] L. Chen, P. Chen, H. Wang, W. Cui, J. Sheng, J. Li, Y. Zhang, Y. Zhou, F. Dong, Surface lattice oxygen activation on $Sr_2Sb_2O_7$ enhances the photocatalytic mineralization of toluene: from reactant activation, intermediate conversion to product desorption, ACS Appl. Mater. Interfaces 13 (2021) 5153–5164.

[144] Z. Lin, X. Tong, W. Shen, J.-C. Roux, H. Xi, Humidity impact on photo-catalytic degradation: adsorption behavior simulations and catalytic reaction mechanisms for main gaseous pollutants in papermaking industry, J. Cleaner Prod. 244 (2020), 118863.

[145] V. Binas, V. Stefanopoulos, G. Kiriakidis, P. Papagiannakopoulos, Photocatalytic oxidation of gaseous benzene, toluene and xylene under UV and visible irradiation over Mn-doped TiO_2 nanoparticles, J. Materiomics 5 (2019) 56–65.

[146] M. Wang, J. Hua, Y. Yang, Fabrication of CDs/CdS-TiO_2 ternary nano-composites for photocatalytic degradation of benzene and toluene under visible light irradiation, Spectrochim. Acta A Mol. Biomol. Spectrosc. 199 (2018) 102–109.

[147] H. Zhuang, Q. Gu, J. Long, H. Lin, H. Lin, X. Wang, Visible light-driven decomposition of gaseous benzene on robust Sn^{2+}-doped anatase TiO_2 nanoparticles, RSC Adv. 4 (2014) 34315–34324.

[148] H. Huang, H. Huang, Y. Zhan, G. Liu, X. Wang, H. Lu, L. Xiao, Q. Feng, D.Y. C. Leung, Efficient degradation of gaseous benzene by VUV photolysis combined with ozone-assisted catalytic oxidation: performance and mechanism, Appl. Catal. B 186 (2016) 62–68.

[149] V.V. Kislov, T.L. Nguyen, A.M. Mebel, S.H. Lin, S.C. Smith, Photodissociation of benzene under collision-free conditions: an abinitio/Rice-Ramsperger-Kassel-Marcus study, J. Chem. Phys. 120 (2004) 7008–7017.

[150] J. Li, X.a. Dong, G. Zhang, W. Cui, W. Cen, Z. Wu, S.C. Lee, F. Dong, Probing ring-opening pathways for efficient photocatalytic toluene decomposition, J. Mater. Chem. A 7 (2019) 3366-3374.

[151] P. Chen, W. Cui, H. Wang, X. Dong, J. Li, Y. Sun, Y. Zhou, Y. Zhang, F. Dong, The importance of intermediates ring-opening in preventing photocatalyst deactivation during toluene decomposition, Appl. Catal. B 272 (2020), 118977.

[152] J. Li, K. Li, B. Lei, M. Ran, Y. Sun, Y. Zhang, K.-H. Kim, F. Dong, High-efficiency photocatalytic decomposition of toluene over defective InOOH promotive role of oxygen vacancies in ring opening process, Chem. Eng. J. 413 (2021), 127389.

[153] F. Liu, C.-X. Xiao, L.-H. Meng, L. Chen, Q. Zhang, J.-B. Liu, S. Shen, J.-K. Guo, C.-T. Au, S.-F. Yin, Facile fabrication of octahedral CdS-ZnS by cation exchange for photocatalytic toluene selective oxidation, ACS Sustain. Chem. Eng. 8 (2020) 1302–1310.

[154] H. Mohan, J.M. Lim, S.W. Lee, J.S. Jang, Y.J. Park, K.K. Seralathan, B.T. Oh, Enhanced visible light photocatalysis with E-waste-based V_2O_5/zinc-ferrite: BTEX degradation and mechanism, J. Chem. Technol. Biotechnol. 6442 (2020).

[155] M. Hinojosa-Reyes, S. Arriaga, L.A. Diaz-Torres, V. Rodríguez-González, Gas-phase photocatalytic decomposition of ethylbenzene over perlite granules coated with indium doped TiO_2, Chem. Eng. J. 224 (2013) 106–113.

[156] Z. Cheng, P. Sun, Y. Jiang, J. Yu, J. Chen, Ozone-assisted UV_{254nm} photodegradation of gaseous ethylbenzene and chlorobenzene: effects of process parameters, degradation pathways, and kinetic analysis, Chem. Eng. J. 228 (2013) 1003–1010.

[157] Y. Meng, T. Dai, X. Zhou, G. Pan, S. Xia, Photodegradation of volatile organic compounds catalyzed by MCr-LDHs and hybrid MO@MCr-LDHs (M = Co, Ni, Cu, Zn): the comparison of activity, kinetics and photocatalytic mechanism, Catal. Sci. Technol. 10 (2020) 424–439.

[158] Y. Shu, Y. Xu, H. Huang, J. Ji, S. Liang, M. Wu, D.Y.C. Leung, Catalytic oxidation of VOCs over Mn/TiO_2/activated carbon under 185nm VUV irradiation, Chemosphere 208 (2018) 550–558.

[159] L. Mohan V, S.M. Shiva Nagendra, M.P. Maiya, Photocatalytic degradation of gaseous toluene using self-assembled air filter based on chitosan/activated carbon/TiO_2, J. Environ. Chem. Eng. 7 (2019) 103454-103455.

[160] J. Kim, B.-K. Lee, Enhanced photocatalytic decomposition of VOCs by visible-driven photocatalyst combined Cu-TiO_2 and activated carbon fiber, Process Saf. Environ. Prot. 119 (2018) 164–171.

[161] M. Li, B. Lu, Q.F. Ke, Y.J. Guo, Y.P. Guo, Synergetic effect between adsorption and photodegradation on nanostructured TiO_2/activated carbon fiber felt porous composites for toluene removal, J. Hazard. Mater. 333 (2017) 88–98.

[162] Q. Chen, L. Liu, L. Liu, Y. Zhang, A novel UV-assisted PEC-MFC system with CeO_2/TiO_2/ACF catalytic cathode for gas phase VOCs treatment, Chemosphere 126930 (2020).

[163] H. Huang, H. Huang, Q. Feng, G. Liu, Y. Zhan, M. Wu, H. Lu, Y. Shu, D.Y.C. Leung, Catalytic oxidation of benzene over Mn modified TiO_2/ZSM-5 under vacuum UV irradiation, Appl. Catal. B 203 (2017) 870–878.

[164] H. Huang, G. Liu, Y. Zhan, Y. Xu, H. Lu, H. Huang, Q. Feng, M. Wu, Photocatalytic oxidation of gaseous benzene under VUV irradiation over TiO_2/Zeolites catalysts, Catal. Today 281 (2017) 649–655.

[165] W. Abou Saoud, A.A. Assadi, A. Kane, A.-V. Jung, P. Le Cann, A. Gerard, F. Bazantay, A. Bouzaza, D. Wolbert, Integrated process for the removal of indoor VOCs from food industry manufacturing: elimination of butane-2,3-dione and heptan-2-one by cold plasma-photocatalysis combination, J. Photochem. Photobiol. A 386 (2020), 112071.
[166] A.A. Assadi, J. Palau, A. Bouzaza, J. Penya-Roja, V. Martinez-Soriac, D. Wolbert, Abatement of 3-methylbutanal and trimethylamine with combined plasma and photocatalysis in a continuous planar reactor, J. Photochem. Photobiol. A 282 (2014) 1–8.
[167] T. Zhu, R. Chen, N. Xia, X. Li, X. He, W. Zhao, T. Carr, Volatile organic compounds emission control in industrial pollution source using plasma technology coupled with F-TiO_2/gamma-Al_2O_3, Environ. Technol. 36 (2015) 1405–1413.
[168] J. Ma, J. Wang, Y. Dang, Photo-assisted oxidation of gaseous benzene on tungsten-doped MnO_2 at lower temperature, Chem. Eng. J. 388 (2020), 124387.
[169] J. Li, S. Cai, E. Yu, B. Weng, X. Chen, J. Chen, H. Jia, Y. Xu, Efficient infrared light promoted degradation of volatile organic compounds over photo-thermal responsive Pt-rGO-TiO_2 composites, Appl. Catal. B 233 (2018) 260–271.
[170] J. Li, E. Yu, S. Cai, X. Chen, J. Chen, H. Jia, Y. Xu, Noble metal free, CeO_2/$LaMnO_3$ hybrid achieving efficient photo-thermal catalytic decomposition of volatile organic compounds under IR light, Appl. Catal. B 240 (2019) 141–152.
[171] C. Jiang, H. Wang, Y. Wang, C. Xue, Z. Yang, C. Yu, H. Ji, Modifying defect States in CeO_2 by Fe doping: a strategy for low-temperature catalytic oxidation of toluene with sunlight, J. Hazard. Mater. 390 (2020), 122182.
[172] S. Weon, W. Choi, TiO_2 nanotubes with open channels as deactivation-resistant photocatalyst for the degradation of volatile organic compounds, Environ. Sci. Technol. 50 (2016) 2556–2563.
[173] A.H. Mamaghani, F. Haghighat, C.-S. Lee, Photocatalytic oxidation technology for indoor environment air purification: the state-of-the-art, Appl. Catal. B 203 (2017) 247–269.
[174] Y.T. Wu, Y.H. Yu, V.H. Nguyen, K.T. Lu, J.C. Wu, L.M. Chang, C.W. Kuo, Enhanced xylene removal by photocatalytic oxidation using fiber-illuminated honeycomb reactor at ppb level, J. Hazard. Mater. 262 (2013) 717–725.